

1           **Dynamic proton-dependent motors power Type IX secretion and gliding adhesin**  
2   **movement in *Flavobacterium***

3  
4  
5 Maxence S. Vincent<sup>1,†</sup>, Caterina Comas Hervada<sup>1</sup>, Corinne Sebban-Kreuzer<sup>1</sup>, Hugo Le  
6 Guenno<sup>2</sup>, Maïalène Chabalier<sup>1</sup>, Artemis Kosta<sup>2</sup>, Françoise Guerlesquin<sup>1</sup>, Tâm Mignot<sup>3</sup>, Mark  
7 McBride<sup>4</sup>, Eric Cascales<sup>1,\*</sup>, Thierry Doan<sup>1,\*</sup>

8  
9 <sup>1</sup>Laboratoire d'Ingénierie des Systèmes Macromoléculaires, Institut de Microbiologie, Bioénergies et  
10 Biotechnologie, Aix-Marseille Université – CNRS UMR7255, 31 Chemin Joseph Aiguier, CS7071,  
11 13402 Marseille Cedex 09, France

12  
13 <sup>2</sup>Microscopy Core Facility, Institut de Microbiologie, Bioénergies et Biotechnologie, FR3479, Aix-  
14 Marseille Université – CNRS UMR7283, 31 Chemin Joseph Aiguier, CS7071, 13402 Marseille Cedex  
15 09, France

16  
17 <sup>3</sup>Laboratoire de Chimie Bactérienne, Institut de Microbiologie, Bioénergies et Biotechnologie, Aix-  
18 Marseille Université – CNRS UMR7283, 31 Chemin Joseph Aiguier, CS7071, 13402 Marseille Cedex  
19 09, France

20  
21 <sup>4</sup>Department of Biological Sciences, University of Wisconsin – Milwaukee, Milwaukee, Wisconsin,  
22 USA

23  
24  
25  
26 \* To whom correspondence should be addressed. Email: [tdoan@imm.cnrs.fr](mailto:tdoan@imm.cnrs.fr), [cascales@imm.cnrs.fr](mailto:cascales@imm.cnrs.fr)

27  
28 † Current address: Department of Biochemistry, University of Oxford, South Parks Road, Oxford OX1  
29 3QU, U.K.

30  
31  
32 Running title: GldLM proton channels drive Type IX secretion and gliding motility  
33  
34

35 **Abstract**

36

37 Motile bacteria usually rely on external apparatus like flagella for swimming or pili for  
38 twitching. By contrast, gliding bacteria do not rely on obvious surface appendages to move on  
39 solid surfaces. *Flavobacterium johnsoniae* and other bacteria in the Bacteroidetes phylum use  
40 adhesins whose movement on the cell surface supports motility. In *F. johnsoniae*, secretion and  
41 helicoidal motion of the main adhesin SprB are intimately linked and depend on the type IX  
42 secretion system (T9SS). Both processes necessitate the proton motive force (PMF), which is  
43 thought to fuel a molecular motor that comprises the GldL and GldM cytoplasmic membrane  
44 proteins. Here we show that *F. johnsoniae* gliding motility is powered by the pH gradient  
45 component of the PMF. We further delineate the interaction network between the GldLM  
46 transmembrane helices (TMH) and show that conserved glutamate residues in GldL TMH are  
47 essential for gliding motility, although having distinct roles in SprB secretion and motion. We  
48 then demonstrate that the PMF and GldL trigger conformational changes in the GldM  
49 periplasmic domain. We finally show that multiple GldLM complexes are distributed in the  
50 membrane suggesting that a network of motors may be present to move SprB along a helical  
51 path on the cell surface. Altogether, our results provide evidence that GldL and GldM assemble  
52 dynamic membrane channels that use the proton gradient to power both T9SS-dependent  
53 secretion of SprB and its motion at the cell surface.

54

55

56

## 57 **Introduction**

58 *Flavobacterium johnsoniae*, one of the fastest gliding bacteria described to date, uses surface-  
59 anchored adhesins to move on solid surfaces (Nelson, Bollampalli et al. 2008, Shrivastava,  
60 Rhodes et al. 2012, Nan, McBride et al. 2014). Remarkably, the major adhesin SprB exhibits a  
61 rotational behavior (Shrivastava, Lele et al. 2015) and its motion at the cell surface describes a  
62 closed helicoidal pattern along the long axis of the cell (Nakane, Sato et al. 2013, Shrivastava,  
63 Roland et al. 2016). It is proposed that binding of SprB to the substratum generates adhesion  
64 points and hence that SprB motion relative to the cell displaces the cell body in a forward screw-  
65 like motion (Shrivastava, Roland et al. 2016, Wadhwa and Berg 2021). SprB and other adhesins  
66 involved in gliding motility are transported to the cell surface by a multiprotein secretion  
67 apparatus, named type IX secretion system (T9SS) (Rhodes, Samarasam et al. 2010,  
68 Shrivastava, Johnston et al. 2013, Kulkarni, Johnston et al. 2019), which is present in most  
69 bacteria in the Bacteroidetes phylum (McBride and Zhu 2013, Abby, Cury et al. 2016).

70 The T9SS was discovered in the opportunistic pathogen *Porphyromonas gingivalis* in which it  
71 conveys a large number of virulence factors, including gingipain proteinases, across the outer  
72 membrane (OM) to the cell surface or the extracellular milieu (Sato, Naito et al. 2010, Goulas,  
73 Mizgalska et al. 2015, Nakayama 2015). In addition to gliding adhesins and gingipain  
74 proteinases, the repertoire of T9SS substrates also includes enzymes involved in nutrient supply  
75 and biofilm formation (Sato, Naito et al. 2010, Kharade and McBride 2014, Tomek, Neumann  
76 et al. 2014, Kita, Shibata et al. 2016). While the roles of the T9SSs and their substrates are  
77 relatively well known, information on T9SS architecture and mechanism of action are still  
78 sparse. However, conserved features of the T9SS have recently emerged (Lasica, Ksiazek et al.  
79 2017, McBride 2019, Gorasia, Veith et al. 2020, Lunar Silva and Cascales 2021). The common  
80 T9SS architecture includes (i) the trans-envelope complex GldKLMN composed of two inner  
81 membrane (IM) proteins, GldL (or PorL) and GldM (or PorM), and of an OM-associated ring  
82 complex composed of the GldK OM lipoprotein and the GldN periplasmic protein (Gorasia,  
83 Veith et al. 2016, Vincent, Canestrari et al. 2017, Leone, Roche et al. 2018), (ii) the SprA (or  
84 Sov) OM translocon (Lauber, Deme et al. 2018), and (iii) the attachment complex that is  
85 comprised of the PorU, PorV and PorZ proteins (Chen, Peng et al. 2011, Glew, Veith et al.  
86 2012, Gorasia, Veith et al. 2015, Glew, Veith et al. 2017, Madej, Nowakowska et al. 2021).  
87 These proteins assemble through a dense network of interactions that are poorly characterized  
88 and likely involve other conserved T9SS subunits.

89 T9SS-dependent secretion and gliding motility is a process energized by the IM proton-motive  
90 force (PMF) because inhibitors that dissipate the PMF prevent substrate secretion and halt cell

91 displacement (Ridgway 1977, Pate and Chang 1979, Duxbury, Humphrey et al. 1980, Dzink-  
92 Fox, Leadbetter et al. 1997). At the single-cell level, Nakane and colleagues directly observed  
93 that SprB dynamics halted almost immediately after the addition of carbonyl cyanide *m*-  
94 chlorophenyl hydrazone (CCCP), a protonophore that collapses the PMF (Nakane, Sato et al.  
95 2013). Hence, it was proposed that a PMF-dependent motor powers SprB dynamics and cell  
96 gliding. The nature of the molecular motor that powers SprB motion has been a longstanding  
97 question. Among the T9SS core components, only the GldL and GldM IM proteins share  
98 features with recognized PMF-dependent motors involved in the energization of flagellum  
99 rotation (MotAB), iron acquisition (ExbBD), outer membrane stability (TolQR), or myxococcal  
100 gliding motility and sporulation (AglQRS) (Block and Berg 1984, Skare and Postle 1991,  
101 Bradbeer 1993, Cascales, Llobès et al. 2001, Sun, Wartel et al. 2011, Wartel, Ducret et al.  
102 2013). GldL presents two transmembrane helices (TMHs) and largely faces the cytoplasm while  
103 GldM is a bitopic protein with a large periplasmic C-terminal domain. The *P. gingivalis*  
104 homologs of GldL and GldM (PorL and PorM, respectively) interact via their TMHs (Vincent,  
105 Canestrari et al. 2017). In addition, structural studies showed that the GldM and PorM  
106 periplasmic regions form dimers, and are composed of four domains, from D1 to D4 (Leone,  
107 Roche et al. 2018). The C-terminal D4 domain of PorM is involved in interactions with the  
108 outer membrane-associated PorKN complex (Leone, Roche et al. 2018). Finally, GldL/PorL  
109 and GldM/PorM bear conserved glutamate residues that may participate in harvesting the PMF  
110 (Vincent, Canestrari et al. 2017, McBride 2019). GldL and GldM are thus ideal candidates for  
111 constituting the IM proton-dependent motor powering type IX secretion and/or SprB dynamics.  
112 Indeed, a recent study presented the cryo-electron microscopy structure of the GldLM complex  
113 (Hennell James, Deme et al. 2021). The complex comprises two single transmembrane helices  
114 of GldM inside a pentameric ring of GldL, an architecture common with other known motors.  
115 The study also provided evidence that inter-TMH contacts modulated by the PMF are important  
116 for motor function. In addition, protonatable residues located in the GldL TMHs were shown  
117 to be essential for motor function (Hennell James, Deme et al. 2021). Here we provide further  
118 support and expand these conclusions. We show that the proton gradient component of the PMF  
119 is the source of energy powering gliding motility. We further demonstrate that the function of  
120 the GldLM motor requires a highly conserved glutamate residue in GldL, E49, whose  
121 protonation state controls interactions between the GldL and GldM TMHs and GldM  
122 conformation. We then show that substitution of a second GldL glutamate residue, E59, had no  
123 effect on secretion of SprB to the cell surface, but abolished SprB movement, thereby  
124 constituting a tool to uncouple T9SS-dependent secretion and gliding motility. Based on these

125 results, we propose an updated model in which GldM conformational change upon PMF  
126 sensing is transmitted into mechanical torque through the periplasmic part of the T9SS to drive  
127 SprB motion.

128

## 129 **Results and Discussion**

### 130 **Gliding is energized by the proton gradient**

131 It is well known that gliding motility is arrested upon dissipation of the proton-motive force  
132 (Ridgway 1977, Pate and Chang 1979, Duxbury, Humphrey et al. 1980, Dzink-Fox, Leadbetter  
133 et al. 1997). The PMF consists of two gradients across the cytoplasmic membrane: an electrical  
134 potential ( $\Delta\psi$ ) and a chemical potential ( $\Delta\text{pH}$ ). To better define the energy source that powers  
135 gliding motility, *F. johnsoniae* gliding cells in a well chamber with glass bottom were subjected  
136 to valinomycin/ $\text{K}^+$  or nigericin, to specifically dissipate  $\Delta\psi$  or  $\Delta\text{pH}$  respectively, and single-  
137 cell gliding motility was quantified (Fig. 1A and B). In agreement with previous observations  
138 (Nakane, Sato et al. 2013), cells glide with an average speed of  $1.7 \mu\text{m}\cdot\text{s}^{-1}$  (Fig. 1B). As a  
139 control, injection of  $10 \mu\text{M}$  of CCCP rapidly blocked all cell displacement in a reversible  
140 manner. By contrast, no significant inhibitory effect was observed upon addition of  $40 \mu\text{M}$   
141 valinomycin ( $+50 \text{ mM KCl}$ ). However, when cells were treated with  $7 \mu\text{M}$  nigericin, motility  
142 was strongly impaired (Fig. 1B). Instead of gliding, cells appeared to jiggle around the same  
143 location, possibly because nigericin did not totally abolish the  $\Delta\text{pH}$  (Fig. 1A). When nigericin  
144 was washed out, cells resumed gliding motility at normal speed. Therefore, we conclude that  
145 the proton gradient, but not the electrical potential, is the source of energy used by the gliding  
146 machinery.

147

### 148 **GldL and GldM constitute the molecular motor that couples PMF to GldM** 149 **conformational changes**

150 Bacterial molecular motors such as the MotAB flagellar stator, the ExbBD and TolQR related  
151 transport systems and the AglRQS gliding motor generate mechanical energy by harvesting the  
152 chemical gradient through the cytoplasmic membrane (Blair and Berg 1990, Ahmer, Thomas  
153 et al. 1995, Cascales, Gavioli et al. 2000, Sun, Wartel et al. 2011). These complexes usually  
154 comprise two subunits organized in a 5:2 stoichiometry that interact via their TMHs (Celia,  
155 Botos et al. 2019, Santiveri, Roa-Eguiara et al. 2020). A conserved acidic residue, located in  
156 one TMH and facing the other TMHs, plays a key role in proton transit (Togashi, Yamaguchi  
157 et al. 1997, Zhou, Sharp et al. 1998, Celia, Noinaj et al. 2016, Celia, Botos et al. 2019, Santiveri,

158 Roa-Eguiara et al. 2020). It is proposed that proton flow through the channel triggers  
159 protonation-deprotonation cycles of the side-chain of this residue and induces rearrangements  
160 in the TMHs, ultimately leading to the production of mechanical torque in the form of  
161 conformational changes in the extramembrane regions (Larsen, Thomas et al. 1999, Germon,  
162 Ray et al. 2001, Kojima and Blair 2001).

163

164 *GldL and GldM interact via their transmembrane segments* – In agreement with the recent  
165 cryo-EM structure of the GldLM complex, bacterial two-hybrid analyses show that GldL and  
166 GldM interact (Fig. 2A). As previously shown for the *P. gingivalis* PorLM complex (Vincent,  
167 Canestrari et al. 2017), these interactions likely involve the transmembrane segments of both  
168 proteins, as GldLM complex formation is prevented when only the soluble domains of these  
169 proteins are tested (Fig. 2A). Finally, similarly to the *P. gingivalis* PorKLMN complex, the  
170 GldLM module is implicated in interactions with the putative outer membrane-associated  
171 GldKN/O ring (Supplementary Fig. S1A) via contacts between the GldM periplasmic domain  
172 and GldK, GldN and GldO (Supplementary Fig. S1B). To test the contribution of TMHs to  
173 GldLM interactions, we conducted GALLEX and BLA approaches. GALLEX is based on the  
174 repression of a  $\beta$ -galactosidase reporter by two LexA DNA binding domains with different  
175 DNA binding specificities (LexA<sup>WT</sup> and LexA<sup>408</sup>). If two TMHs interact, LexA<sup>WT</sup> and LexA<sup>408</sup>  
176 heterodimeric association causes repression of  $\beta$ -galactosidase synthesis (Schneider and  
177 Engelman 2003, Logger, Zoued et al. 2017). We tested interactions between TMHs displaying  
178 *in-to-out* topologies (GldL-TMH1 and GldM-TMH; Fig. 2B). GldL-TMH1 and GldM-TMH  
179 specifically formed homodimers but no interaction was detected between GldL-TMH1 and  
180 GldM TMH (Fig. 2C). To test the interaction with GldL-TMH2, which exhibits an *out-to-in*  
181 topology, we used the BLA assay (Julius, Laur et al. 2017, Schanzenbach, Schmidt et al. 2017).  
182 GldL-TMHs and GldM-TMH were fused to either the N- or C-terminal domain of  $\beta$ -lactamase  
183 (Bla). If an interaction between TMHs occurs, a functional  $\beta$ -lactamase is reconstituted and its  
184 activity can be quantified using a chromogenic substrate-based assay. In this assay, GldL-  
185 TMH2 homodimerization was not observed. However, GldL-TMH2 specifically interacted  
186 with both GldL-TMH1 and GldM-TMH (Fig. 2D). Taken together, our data show that GldL  
187 TMH1 and TMH2 interact with each other and GldL TMH2 interacts with GldM single TMH  
188 in the motor complex. With the exception of GldL-TMH1/GldL-TMH1 contacts detected by  
189 GALLEX, these data are in agreement with the position of the TMHs in the recent cryo-EM  
190 structure of the GldLM complex (Hennell James, Deme et al. 2021).



191

192 *GldM changes conformation depending on the proton gradient* – We next sought to understand  
193 how the GldLM complex responds to the proton gradient. Our previous structural  
194 characterization of GldM and its homolog PorM from *P. gingivalis* revealed a conformational  
195 flexibility in the periplasmic region of GldM (Leone, Roche et al. 2018). The extracellular  
196 domain of GldM forms a straight homodimer that spans most of the periplasm. Each monomer  
197 is composed of four domains, D1 to D4 (Leone, Roche et al. 2018, Sato, Okada et al. 2020).  
198 Interestingly, the homolog PorM presents a kink between domains D2 and D3 (Leone, Roche  
199 et al. 2018), while a kink between the GldM D1 and D2 domains has been revealed in the cryo-  
200 EM structure (Hennell James, Deme et al. 2021), suggesting that GldM/PorM may alternate  
201 between several conformational states. Indeed, recent proteolytic susceptibility assays showed  
202 that the PMF regulates conformational changes in GldM: upon PMF dissipation by CCCP, two  
203 cleavages at the interface of domains D2 and D3 were identified by mass spectrometry after  
204 limited trypsinolysis (Song, Perpich et al. 2021). Here, we extend these observations by  
205 showing that the *in vivo* conformation of GldM is altered by drugs that perturb the proton  
206 gradient such as CCCP and nigericin, but remained unaffected upon treatment with the F<sub>1</sub>F<sub>0</sub>  
207 ATPase inhibitors sodium azide and sodium arsenate, nor upon dissipation of the  $\Delta\psi$  by  
208 valinomycin (Fig. 3A), demonstrating that GldM undergoes a structural transition dependent  
209 on the IM proton gradient (Fig. 3B).

210

211 *A conserved glutamate residue in GldL TMH2 is critical for harvesting the proton gradient* –  
212 The activity of bacterial MotAB-like molecular motors characterized so far depends on  
213 conserved acidic residues located in their TMHs (Braun, Gaisser et al. 1996, Zhou, Sharp et al.  
214 1998, Cascales, Lloubès et al. 2001, Sun, Wartel et al. 2011). We first tested the effect of the  
215 drug N-N'-Dicyclohexyl-carbodiimide (DCCD), which covalently reacts with carboxylic groups  
216 located in a hydrophobic environment (Khorana 1953). Addition of DCCD abrogated gliding  
217 motility (Fig. 4A and B) and had the same effect on GldM conformation as CCCP (Fig. 4C).  
218 This effect was irreversible since DCCD remains covalently bound (Fig. 4B). These results  
219 therefore suggested that aspartate or glutamate residues are involved in coupling PMF to GldM  
220 conformational change and gliding motility. Sequence alignment showed that three acidic  
221 residues are conserved in the GldL and GldM N-terminal regions (Supplementary Fig. S2A and  
222 S2B): a glutamate at position 31 in the GldM TMH (GldM-E31) and two glutamates in GldL,  
223 one located in TMH2 (E49; strictly conserved in all GldL homologs in the OrthoDB database),  
224 and one located between TMH2 and the cytoplasmic domain (E59) (Supplementary Fig. S2C).

225 Substitution of GldM E31 (GldM<sup>E31A</sup>) did not exhibit any defect in gliding motility compared  
226 to wild-type GldM, indicating that this residue does not play a significant role in T9SS-  
227 dependent secretion or gliding (Fig. 4D). By contrast, cells producing GldL<sup>E49A</sup> failed to adhere  
228 to the glass surface, while substitution of GldL E59 abolished gliding motility without affecting  
229 adherence (i.e., SprB secretion by the T9SS) (Fig. 4E). Interestingly, the GldL<sup>E49A</sup> and GldL<sup>E59A</sup>  
230 variants presented distinct phenotypes regarding SprB secretion and dynamics as shown by  
231 live-cell immunolabelling using polyclonal anti-SprB antibodies and fluorescence time-lapse  
232 microscopy on agarose pads. As previously reported (Nakane, Sato et al. 2013), wild-type cells  
233 exhibited surface-exposed SprB fluorescent foci that describe an overall helicoidal pattern  
234 along the long cell axis, with dispersed velocity in the order of 1  $\mu\text{m}\cdot\text{s}^{-1}$  (Fig. 4F). No fluorescent  
235 focus was observed in  $\Delta\text{gldL}$  mutant cells, which are unable to secrete SprB, indicating that  
236 SprB immunolabeling was specific. A similar observation was made with  $\text{gldL}^{\text{E49A}}$  mutant cells  
237 (Fig. 4F), demonstrating that T9SS-dependent SprB secretion to the cell surface requires  
238 residue E49 in GldL TMH2. By contrast, the GldL<sup>E59A</sup> substitution supported SprB secretion  
239 but abolished the dynamic cell-surface movements of the adhesin (Fig. 4F-G). It is noteworthy  
240 that all GldL and GldM variants were produced in *F. johnsoniae* at levels comparable to the  
241 wild-type proteins (Supplementary Fig. S2D and S2E), although GldL<sup>E49A</sup> migrated with lower  
242 apparent size than the wild-type protein (Supplementary Fig. S2E), an aberrant migration  
243 already observed in a separate study (Hennell James, Deme et al. 2021) and likely caused by  
244 the difference in detergent binding in SDS-PAGE between the TMH2 variants (Rath,  
245 Glibowicka et al. 2009). Taken together, these results support a model in which GldL E49 is  
246 required for secretion of the SprB adhesin and constitutes a key determinant of T9SS, whereas  
247 GldL E59 is dispensable for secretion and plays a specific function in gliding because it is only  
248 required for SprB movement. We next tested the contribution of these acidic residues for the  
249 regulation of GldM conformation. Protease accessibility assays showed that GldL and its Glu49  
250 residue are required to maintain GldM in the conformation required for T9SS activity (Fig. 4H).  
251 By contrast, the GldL E59A substitution did not impact GldM proteolytic susceptibility (Fig.  
252 4H), suggesting that the GldM conformation change observed by limited proteolysis is  
253 specifically linked to gliding motility rather than effector secretion.

254 *Protonation of GldL glutamate residues* – To address the question whether GldL E49 and E59  
255 residues undergo protonation and deprotonation cycles, we determined their pKa values. A  
256 <sup>15</sup>N/<sup>13</sup>C Glu-labeled synthetic peptide corresponding to GldL TMH2 (L2, residues Val40 to  
257 Val61) was solubilized in deuterated dodecylphosphorylcholine (DPC) micelles and analyzed



258 by NMR. pKa values of  $5.54 \pm 0.04$  and  $5.65 \pm 0.13$  for the carboxylic groups of residues E49  
259 and E59, respectively, were measured by the pH-dependent chemical shifts in two-dimensional  
260  $^{13}\text{C}$ -HSQC experiments (Fig. 5A-B). In the presence of peptides corresponding to GldL TMH1  
261 (L1, residues Lys6 to Thr29) and GldM TMH (M, residues Leu15 to Leu38), the pKa values  
262 slightly increased to  $5.83 \pm 0.02$  for both glutamates (Fig. 5B). The behavior of the  $^{13}\text{C}$  chemical  
263 shifts for the GldL TMH2 glutamate residues was then monitored in presence of the different  
264 peptides. At pH 5.2 (i.e., protonated glutamates), we observed chemical shift variations in the  
265 presence of L1, M or both (Fig. 5C). These data confirm that GldL TMH2 interacts with GldL-  
266 TMH1 and GldM-TMH, and that the presence of these TMH peptides influences the  
267 environment of the glutamate residues. However, at pH 6.7 (i.e., deprotonated glutamates), no  
268 chemical shift was observed upon addition of the L1, M or both peptides (Fig. 5C), suggesting  
269 that GldL TMH1 and GldM TMH are not in the environment of the glutamate residues. Taken  
270 together, these results suggest that the protonation state of the glutamic acids regulates contacts  
271 between TMH2 and the other TMHs in the GldLM complex, and hence that GldLM helix  
272 organization is likely to be modified during motor function, as evidenced for the MotAB and  
273 TolQR motors (Kim, Price-Carter et al. 2008, Zhang, Goemaere et al. 2009).  
274 Altogether our results support a model in which GldL and GldM form an IM proton channel  
275 with conserved critical glutamates that are protonated and deprotonated in response to the  
276 proton gradient to power both T9SS-dependent secretion and gliding motility. Our results also  
277 demonstrate that the protonation state of GldL E49 controls changes within the GldLM TMHs  
278 packing that are likely transmitted to the GldM periplasmic domain.

279

### 280 **GldLM motors and SprB adhesin do not have the same dynamics.**

281 SprB adhesins follow a closed right-handed helical track at the cell surface (Nakane, Sato et al.  
282 2013, Shrivastava, Roland et al. 2016). Two models have been proposed on how the T9SS  
283 controls SprB motion (Nan, McBride et al. 2014, Shrivastava, Lele et al. 2015). In the first  
284 model, fixed rotary motors may activate treads to which SprB adhesins are connected. In the  
285 second model, SprB adhesins are directly connected to moving GldLM motors. The first  
286 scenario requires a network of motor complexes along the SprB helicoidal path. The second  
287 scenario implies that SprB colocalizes with dynamic GldLM complexes, and that SprB and  
288 GldLM move concomitantly along the helicoidal path. To explore these possibilities, we  
289 characterized the localization of the GldLM motor complex. Structured-illumination  
290 microscopy (SIM) recordings of *F. johnsoniae* fixed and permeabilized cells immunolabeled  
291 with polyclonal primary antibodies against the GldL, GldM, GldK or GldN proteins and

292 fluorescent secondary antibodies showed that each protein was distributed in many foci along  
293 the cell body (Fig. 6A). For example, we numbered 32 GldL foci per cell in average (n=11, Fig.  
294 6A). These data suggest that multiple Gld motors decorate the cell envelope. To provide further  
295 information, we sought to perform live observations. However, none of the plasmid-borne or  
296 chromosomal fluorescent fusions to GldL or GldM we generated supported wild-type gliding,  
297 possibly due to the size of the fluorescent protein tags. We therefore turned to a more  
298 sophisticated method to generate functional and time-trackable proteins, using the alfa  
299 technology (Götzke, Kilisch et al. 2019).

300 The alfatag is a 13-amino-acid peptide that is specifically and almost irreversibly bound by the  
301 NBalfa nanobody with an affinity of ~0.26 pM (Götzke, Kilisch et al. 2019). The sequence  
302 encoding the alfatag was introduced in frame with the GldL-coding sequence at the native locus.  
303 GldL-alfa was functional and supported single-cell gliding (Fig. S3A-B). We then engineered  
304 a replicative plasmid expressing NBalfa-sfGFP under the control of an IPTG-inducible  
305 promoter in *F. johnsoniae*. Expression of NBalfa-sfGFP did not perturb cell gliding, either in a  
306 wild-type background or in a strain expressing GldL-alfa (Supplementary Fig. S3B). NBalfa-  
307 sfGFP was diffuse in wild-type cells that do not express GldL-alfa (Fig. S3C). By contrast,  
308 NBalfa-sfGFP exhibited a punctate pattern in GldL-alfa cells (Fig. 6B). Distinct foci were  
309 visible as well as more patchy signals, rendering quantification difficult. Remarkably, these foci  
310 were not all static relative to the cell, as opposed to the SprA translocon (Lauber, Deme et al.  
311 2018), nor did they behave like SprB adhesins that travel along the entire cell length. Time-  
312 lapse microscopy and kymograph analyses of signal dynamics indicated that some foci remain  
313 static while others moved quickly but at varying speed relative to the cell (Fig. 6B and Movie  
314 S1). In addition, fluorescence recovery after photobleaching (FRAP) experiments in non-  
315 moving cells suggest that GldL-alfa movement was restricted to short distances within the cell  
316 because fluorescent signal could not be recovered over a large bleached cell region (Fig. 6C-  
317 D). These two GldL populations could correspond to GldLM complexes engaged into static  
318 complexes with the OM translocon to secrete substrates, and to free GldL proteins or to GldLM  
319 complexes following a track to energize SprB motion. However, colocalization experiments in  
320 live cells with immunolabeled SprB showed that GldL-alfa and SprB do not follow the same  
321 trajectories (Fig. 6E). These results support the tread model (Nan and Zusman 2016,  
322 Shrivastava and Berg 2020) in which GldLM proton channels convert the proton gradient into  
323 mechanical force to displace or activate treads involved in SprB movement (Fig. 6F).

324

325 **Concluding remarks**

326 In this study, we provided evidence that Type IX Secretion and surface adhesin motion are  
327 energized by a molecular motor fueled by the proton gradient, like the flagellar motor and other  
328 bacterial molecular motors. Our data support the idea that interactions between the  
329 transmembrane helices of GldL and GldM shift in response to the proton flux, eventually  
330 leading to conformation changes in the GldM periplasmic domain. Conserved glutamate  
331 residues in GldL are important in this process but are not equivalent in terms of function. While  
332 amino acid E49 in GldL is essential for secretion through the T9SS as observed by Hennell and  
333 colleagues (Hennell James, Deme et al. 2021), glutamate at position 59 is only required for  
334 gliding, indicating that in *F. johnsoniae*, T9SS secretion itself does not require concomitant  
335 SprB motion along the cell surface. Thus, it is tempting to speculate that secretion and SprB  
336 motion are not supported by the same mechanical rearrangements in GldM, or that SprB motion  
337 may require more mechanical torque than the secretion process. Furthermore, since SprB  
338 motion and secretion are uncoupled in the GldL E59A point mutant, this mutation is an  
339 interesting tool to study secretion independently of gliding in *F. johnsoniae*. Nevertheless,  
340 GldL-E59 is also conserved in non-gliding bacteria like *P. gingivalis*, suggesting that it may  
341 also serve for T9 secretion in other bacteria (Supplementary Fig. S2A).

342 Our data also support the idea that GldM conformational shift upon PMF sensing could be  
343 converted into mechanical torque through the periplasmic part of the T9SS. Indeed, we showed  
344 that GldM periplasmic domain is connected to the T9SS GldKNO subcomplex, similar to the  
345 PorKLMN complex in *P. gingivalis*. Two recent studies help understand how this could work.  
346 First, the structure of the GldLM motor showed that ten GldL TMHs (five GldL molecules)  
347 wrap two GldM TMHs in an asymmetric manner (Hennell James, Deme et al. 2021). It was  
348 proposed that GldM TMHs would rotate within a GldL ring in response to the PMF to generate  
349 mechanical movement of GldM periplasmic domain. These findings are consistent with our  
350 data and provide an explanation for why GldL-E49 is required for motor function. However,  
351 they do not explain the role of E59, which is located outside the membrane in the GldLM  
352 structure (Supplementary Fig. S2C; Hennell James et al., 2021). One may hypothesize that E59  
353 enters the proton channel when GldM rotates. Second, *in situ* PorKN rings were observed by  
354 cryo-electron tomography (Gorasia, Chreifi et al. 2020, Song, Perpich et al. 2021). These rings  
355 may serve to maintain T9SS subcomplexes in close proximity to allow sequential translocation,  
356 maturation and attachment of the substrates (Gorasia, Chreifi et al. 2020). Therefore, an  
357 attractive hypothesis is that GldM conformational changes in response to the proton gradient  
358 could generate mechanical torque for the rotation of GldKNO rings, similar to cogwheels, that  
359 directly or indirectly facilitate secretion of T9SS substrates.

360 Finally, our results are consistent with the "rack and pinion" model proposed by Shrivastava  
361 and Berg to explain how the GldLM complex participates in SprB displacement (Shrivastava  
362 and Berg 2020). Our microscopy data suggest the existence of static GldLM motors, which are  
363 presumably associated with static T9SS translocons, and GldLM complexes that are dynamic  
364 but that move differently than do SprB molecules. These motors could be linked to unidentified  
365 motion treads carrying SprB adhesins.

366  
367

## 368 **Material and Methods**

### 369 **Bacterial strains, media and chemicals**

370 All strains are listed in Table S1. *Escherichia coli* strains DH5 $\alpha$  and BTH101 were used for  
371 cloning procedures and bacterial two-hybrid assay, respectively. *E. coli* cells were grown in  
372 Lysogeny Broth, at 37°C or 28°C. For BACTH experiments, gene expression was induced by  
373 the addition of iso-propyl- $\beta$ -D-thio-galactopyranoside (IPTG, Sigma-Aldrich, 0.5 mM) and  
374 plates were supplemented with 5-bromo-4-chloro-3-indolyl- $\beta$ -D-galactopyranoside (X-Gal,  
375 Eurobio, 40  $\mu\text{g.mL}^{-1}$ ). *F. johnsoniae* CJ1827, a streptomycin-resistant *rpsL2* derivative of  
376 ATCC 17061 (UW101), was used as model micro-organism. *F. johnsoniae* cells were grown  
377 at 28°C in Casitone Yeast Extract (CYE) medium (Agarwal, Hunnicutt et al. 1997) or Motility  
378 Medium (MM) (Liu, McBride et al. 2007) as indicated. For selection and maintenance of the  
379 antibiotic resistance, antibiotics were added to the media at the following concentrations:  
380 erythromycin, 100  $\mu\text{g.mL}^{-1}$ ; streptomycin, 100  $\mu\text{g.mL}^{-1}$ ; tetracycline, 20  $\mu\text{g.mL}^{-1}$ , ampicillin,  
381 100  $\mu\text{g.mL}^{-1}$ , kanamycin, 50  $\mu\text{g.mL}^{-1}$ , chloramphenicol, 40  $\mu\text{g.mL}^{-1}$ . Specific enzyme and  
382 chemicals source were as follows: trypsin (Sigma), Carbonyl cyanide *m*-chlorophenyl  
383 hydrazone (CCCP, Sigma, 10  $\mu\text{M}$ ), nigericin (Nig, Sigma, 7  $\mu\text{M}$ ), valinomycin (Val, Sigma,  
384 40  $\mu\text{M}$ ), sodium azide (Az, Sigma, 1.5 mM), arsenate (Ars, Sigma, 20 mM), *N,N'*-  
385 Dicyclohexylcarbodiimide (DCCD, Sigma, 100  $\mu\text{M}$ ).

386

### 387 **Genetic constructs**

388 All plasmids and oligonucleotide primers used in this study are listed in Table S1. Enzymes for  
389 PCR and cloning were used as suggested by manufacturers.

390 Chromosomal mutants were generated as described (Rhodes, Pucker et al. 2011). The suicide  
391 plasmid designed to generate an in-frame deletion of *gldM* was built as follows. A 2.5 kb

392 fragment containing the region upstream of *gldM* and *gldM* start codon was PCR amplified  
393 using oligonucleotide primers F1- $\Delta$ *gldM* and R1- $\Delta$ *gldM*. This fragment was digested with  
394 *Bam*HI and *Sal*I and inserted into plasmid pRR51 cut with the same restriction enzymes to  
395 generate an intermediate plasmid. A 2.5 kb fragment containing *gldM* stop codon and the region  
396 downstream of *gldM* was PCR amplified using oligonucleotide primers F2- $\Delta$ *gldM* and R2-  
397  $\Delta$ *gldM*. Similarly, it was digested with *Sal*I and *Sph*I and inserted into the previously generated  
398 plasmid cut with *Sal*I and *Sph*I to generate plasmid pRR51- $\Delta$ *gldM*.

399 The suicide plasmids designed to build *gldL*<sup>E49A</sup> and *gldL*<sup>E59A</sup> strains were constructed as  
400 follows. A plasmid with plasmid pRR51 backbone and carrying a 4 kb region centered around  
401 *gldL* E49A and E59A codon substitutions was synthesized (Geneart, Thermofisher). The  
402 suicide plasmid pRR51-*gldL*<sup>E49A</sup> was then built by restoring the codon for E59 in the previously  
403 synthesized plasmid by site directed mutagenesis with oligonucleotide primers Fw-GldL-A59E  
404 and Rv-GldL-A59E. Similarly, the suicide plasmid pRR51-*gldL*<sup>E59A</sup> was built by restoring the  
405 codon for E49 in the previously synthesized plasmid by site directed mutagenesis with  
406 oligonucleotide primers Fw-GldL-A49E and Rv-GldL-A49E.

407 The suicide plasmid used to generate the GldL-alfa fusion was made as follows. A 1.5 kb  
408 fragment containing *gldL* and part of the alfa tag was PCR amplified using oligonucleotide  
409 primers oTM582 and oTM590. A 1.5 kb fragment containing part of the alfa tag, a stop codon  
410 and the region immediately downstream of *gldL* stop codon was PCR amplified using  
411 oligonucleotide primers oTM591 and oTM592. These fragments were assembled using Gibson  
412 isothermal reaction and reamplified using oligonucleotide primers oTM582 and oTM592. This  
413 fragment was digested with *Bam*HI and *Sph*I and inserted into pRR51 cut with the same  
414 restriction enzymes. Plasmids for GALLEX and BLA were engineered by hybridizing  
415 complementary oligonucleotides corresponding to the GldL or GldM TMHs, and inserting them  
416 into *Nhe*I-*Bam*HI-digested target GALLEX or BLA vectors. BACTH plasmids were  
417 engineered by restriction and ligation as previously described (Vincent, Canestrari et al. 2017).  
418 The replicative plasmid designed for complementation and production of GldLM<sup>WT</sup> were  
419 constructed as follows. A fragment containing *gldL* and *gldM* open reading frames was PCR  
420 amplified using oligonucleotide primers 5-*Bam*HI-LM and 3-*Xba*I-LM. This fragment was  
421 digested with *Bam*HI and *Xba*I and inserted into plasmid pCP11 (McBride and Kempf 1996)  
422 cut with the same restriction enzymes. The replicative plasmid designed to produce GldM<sup>E31A</sup>  
423 was then generated by quick change site directed mutagenesis using oligonucleotide primers 5-  
424 GldM-E31A and 3-GLdM-E31A.

425 The replicative plasmid designed to express NbAlfa-sfGFP from an IPTG inducible promoter  
426 in *F. johnsoniae* was designed as follows. A first replicative plasmid was built with an IPTG-  
427 inducible promoter, a multicloning site and *lacI* constitutive expression for repression in the  
428 absence of IPTG in *F. johnsoniae*. A fragment containing the promoter of Fjoh\_0697 (Chen,  
429 Kaufman et al. 2010) with *lacO3* and *lacO1* operator sites flanking the -33 and -7 promoter  
430 sequences, pCP23 multicloning site and Fjoh\_0139 promoter after the *PstI* restriction site was  
431 synthesized (Geneart, Thermofisher). A fragment containing *lacI* open reading frame was PCR  
432 amplified using oligonucleotide primers oTM495 and oTM496. These fragments were  
433 assembled by Gibson isothermal reaction and reamplified using oligonucleotide primers  
434 oTM497 and oTM496. This fragment was digested with *KpnI* and *SphI* and inserted into pCP23  
435 (Agarwal, Hunnicutt et al. 1997) cut with the same restriction enzymes to generate plasmid  
436 pCP-*lac*. Then, the gene encoding NbAlfa was synthesized (Geneart, Thermofisher) and  
437 reamplified using oligonucleotide primers oTM612 and oTM596. sfGFP, codon-optimized for  
438 translation in *F. johnsoniae*, was also synthesized (Geneart, Thermofisher) and then reamplified  
439 by PCR using oligonucleotide primers oTM595 and oTM593. These fragments were assembled  
440 using the Gibson isothermal reaction and reamplified using oligonucleotide primers oTM612  
441 and oTM593. It was then digested with *BamHI* and *NheI* and inserted into plasmid pCP-*lac* cut  
442 with the same restriction enzymes.

#### 443 **Protein interaction assays**

444 The adenylate cyclase-based bacterial two-hybrid technique was used as previously published  
445 (Vincent, Canestrari et al. 2017). Briefly, the proteins to be tested were fused to the isolated  
446 T18 and T25 catalytic domains of the *Bordetella* adenylate cyclase. After introduction of the  
447 two plasmids producing the fusion proteins into the BTH101 reporter strain, plates were  
448 incubated at 28°C for 24 h. Three independent colonies for each transformation were inoculated  
449 into 600 µL of LB medium supplemented with ampicillin, kanamycin, and IPTG (0.5 mM).  
450 After overnight growth at 28°C, 10 µL of each culture was spotted onto LB plates supplemented  
451 with ampicillin, kanamycin, IPTG, and X-Gal and incubated at 28°C. Controls include  
452 interaction assays with TolB and Pal, two protein partners unrelated to the T9SS. The  
453 experiments were done in triplicate and a representative result is shown.  
454 GALLEX and BLA were performed as described (Logger, Zoued et al. 2017).

455

#### 456 **Protease susceptibility assay**



457 *F. johnsoniae* cells were grown in 5 mL of CYE medium to an  $A_{600}=0.8$ , harvested by  
458 centrifugation and resuspended in 100  $\mu\text{L}$  of 20 mM Tris-HCl pH 8.0, 20% sucrose, 1 mM  
459 EDTA, and 100  $\mu\text{g}\cdot\text{mL}^{-1}$  of lysozyme. After 30 min incubation at room temperature (20°C),  
460 100  $\mu\text{L}$  of ice-cold sterile water was added and the mixture was carefully mixed by three  
461 inversions. 50  $\mu\text{L}$  of each spheroplast suspension was treated with trypsin (100  $\mu\text{g}\cdot\text{mL}^{-1}$ ). After  
462 5 min on ice, 17  $\mu\text{L}$  of boiling 4 $\times$  Laemmli loading buffer was added, and immediately vortexed  
463 and boiled for 5 min prior to SDS-PAGE and immunoblot.

464

#### 465 **Western blot analyses**

466 *F. johnsoniae* cells were grown to mid-log phase in CYE at 28°C. Whole cells were prepared  
467 for SDS-PAGE and Western blotting assays were performed as previously described. Equal  
468 amounts of total proteins were loaded for each sample based on culture optical densities. Anti-  
469 GldL, anti-GldM (Shrivastava, Johnston et al. 2013) and anti-FLAG (Sigma Aldrich, clone M2)  
470 antisera were used at 1/5000, 1/5000 and 1/10,000 dilutions, respectively.

471

#### 472 **Nuclear Magnetic Resonance**

473 NMR experiments were carried out on a Bruker Avance III 600 MHz spectrometer, at 300 K.  
474 Three synthetic peptides L1 (GldL-TMH1: KKVMNFAYGMGAAVVIVGALFKITKK), L2  
475 (GldL-TMH2: KKVMLSIGLLTEALIFALSAFEPVKK) and M (GldM-TMH:  
476 KKLMYLVFIAMLAMNVSKEVISAFGLKK), with  $^{15}\text{N}/^{13}\text{C}$ -Glu-labeled, have been studied  
477 free and in complexes at molar ratio 1:1 or 1:1:1. NMR samples containing 1 mM peptide  
478 concentration in 150 mM deuterated DPC were used in different phosphate buffers (50 mM).  
479 The behaviour of the  $^{13}\text{C}$  chemical shifts for glutamate residues in the different peptides as a  
480 function of pH (2.9 to 8.9) was monitored using a two-dimensional  $^{13}\text{C}$ -HSQC experiment.  
481 Chemical shift values as a function of pH were analyzed according to a single titration curve of  
482 the form:

483

484

485

$$\delta = \delta_{HA} - \left( \frac{(\delta_{HA} - \delta_A)}{(1 + 10^{n(pK_a - pH)})} \right)$$

486 where  $\delta$  is the observed chemical shift at a given pH,  $\delta_{HA}$  and  $\delta_A$  are the chemical shifts for the  
487 various protonated forms of the peptide, and  $n$  is the number of protons transferred.

488

#### 489 **Fluorescence microscopy and image analysis**

490 *General microscopy* – For single-cell gliding on glass, cells were grown in CYE at 28°C to an  
491  $A_{600\text{ nm}} \approx 0.7$ . Cells were diluted to an  $A_{600\text{ nm}} \approx 0.05$  and 100  $\mu\text{L}$  were spotted into  $\mu$ -Slide  
492 chambers with glass coverslip bottom (Ibidi). After 5-min incubation, floating cells were  
493 washed out with fresh CYE medium and gliding of adherent cells was monitored by phase  
494 contrast microscopy on a Nikon Eclipse TE-2000 microscope equipped with a 100 $\times$  NA 1.3  
495 Ph3 objective, a perfect focus system to maintain the plane in focus, and an Orcaflash 4.0 LT  
496 digital camera (Hamamatsu Photonics). GldL-alfa/NBalfa-sfGFP localization was observed by  
497 Hilo microscopy. Cells were grown in CYE overnight without shaking at 28°C. NBalfa-sfGFP  
498 expression was induced with 1 mM IPTG for 1 h prior to observation. Cells were spotted on a  
499 2 % low-melting agarose pad for immediate observation. Hilo fluorescence microscopy and  
500 FRAP experiments were performed with a Nikon Eclipse Ti2 microscope equipped with a 100x  
501 NA 1.45 Ph3 objective, an Orca-Fusion digital camera (Hamamatsu), a perfect focus system,  
502 and an Ilas2 TIRF/FRAP module (Gataca Systems).

503 *Immunolabelling and SIM acquisition* – SprB immunolabelling on live cells was performed  
504 essentially as described (Nakane, Sato et al. 2013). Briefly, 500  $\mu\text{L}$  of cells were incubated 5  
505 min with a 1/100 dilution of antiserum directed against SprB (Nelson, Bollampalli et al. 2008).  
506 Cells were washed once with CYE and further incubated 5 min with Alexa488- or Alexa561-  
507 labeled anti-rabbit secondary antibodies (Thermofisher). Cells were washed four times in CYE  
508 and concentrated 5-fold. In order to facilitate SprB detection and tracking during short periods,  
509 cells were spotted on a 2 % low-melting agarose pad for immediate observation.  
510 Immunolabeling of GldL, GldM, GldK and GldN was performed on fixed cells as previously  
511 described (Braun and McBride 2005), except cells were manipulated in tubes instead of on  
512 glass slides. Polyclonal antisera directed against GldL, GldM, GldK or GldN (Shrivastava,  
513 Johnston et al. 2013) were used at 1/2000 dilution and further recognized by Alexa488-labeled  
514 anti-rabbit secondary antibodies (Thermofisher). Structure illumination microscopy (SIM) was  
515 performed on a DeltaVision OMX SR microscope (GE Healthcare). The experiments were done  
516 in triplicate and a representative result is shown.

517 *Image analysis* – Images were analyzed using ImageJ (<http://imagej.nih.gov/ij/>). The MicrobeJ  
518 plugin (Ducret, Quardokus et al. 2016) was used to detect and track cells during gliding. The  
519 Trackmate plugin (Tinevez, Perry et al. 2017) was used to detect SprB fluorescence and analyze  
520 its dynamics. Statistical dataset analysis was performed using Excel and the R software  
521 environment (<https://www.r-project.org/>). Kymographs were generated using the  
522 KymoResliceWide plugin (<https://imagej.net/KymoResliceWide>, E. Katrukha and L. Young).

523 For fluorescence recovery quantification, images were corrected for bleaching using histogram  
524 matching prior to signal recovery quantification.

525

## 526 **Data availability**

527 All data and material are made available upon request.

528

## 529 **Acknowledgements**

530 We thank the members of the Cascales team for insightful discussions and support, Jean-Pierre  
531 Duneau for discussion regarding peptide solubilization, Moly Ba, Isabelle Bringer, Annick  
532 Brun, Olivier Uderso, Mathilde Valade and Audrey Gozzi for technical assistance. This work  
533 was supported by the Aix-Marseille Université (AMU), the Centre National de la Recherche  
534 Scientifique (CNRS), and grants from the Agence Nationale de la Recherche (ANR-15-CE11-  
535 0039 and ANR-20-CE11-0017), from the Excellence Initiative of Aix-Marseille University  
536 (A\*MIDEX, A-M-AAP-ID-17-33-170301-07.22), a French “Investissements d’Avenir”  
537 programme, and from the Fondation Bettencourt-Schueller. M.S.V. was supported by a doctoral  
538 fellowship from the French Ministère de la Recherche, and an end-of-thesis fellowship from  
539 the Fondation pour la Recherche Médicale (FDT2018-05005242).

540

## 541 **References**

- 542 Abby, S. S., J. Cury, J. Guglielmini, B. Néron, M. Touchon and E. P. Rocha (2016).  
543 "Identification of protein secretion systems in bacterial genomes." *Sci Rep* **6**: 23080.  
544 Agarwal, S., D. W. Hunnicutt and M. J. McBride (1997). "Cloning and characterization of the  
545 *Flavobacterium johnsoniae* (Cytophaga johnsonae) gliding motility gene, *gldA*." *Proc Natl*  
546 *Acad Sci U S A* **94**(22): 12139-12144.  
547 Ahmer, B. M., M. G. Thomas, R. A. Larsen and K. Postle (1995). "Characterization of the  
548 *exbBD* operon of *Escherichia coli* and the role of ExbB and ExbD in TonB function and  
549 stability." *J Bacteriol* **177**(16): 4742-4747.  
550 Blair, D. F. and H. C. Berg (1990). "The MotA protein of *E. coli* is a proton-conducting  
551 component of the flagellar motor." *Cell* **60**(3): 439-449.  
552 Block, S. M. and H. C. Berg (1984). "Successive incorporation of force-generating units in the  
553 bacterial rotary motor." *Nature* **309**(5967): 470-472.  
554 Bradbeer, C. (1993). "The proton motive force drives the outer membrane transport of  
555 cobalamin in *Escherichia coli*." *J Bacteriol* **175**(10): 3146-3150.  
556 Braun, T. F. and M. J. McBride (2005). "*Flavobacterium johnsoniae* GldJ is a lipoprotein that  
557 is required for gliding motility." *J Bacteriol* **187**(8): 2628-2637.  
558 Braun, V., S. Gaisser, C. Herrmann, K. Kampfenkel, H. Killmann and I. Traub (1996). "Energy-  
559 coupled transport across the outer membrane of *Escherichia coli*: ExbB binds ExbD and TonB  
560 in vitro, and leucine 132 in the periplasmic region and aspartate 25 in the transmembrane region  
561 are important for ExbD activity." *J Bacteriol* **178**(10): 2836-2845.

562 Cascales, E., M. Gavioli, J. N. Sturgis and R. Lloubès (2000). "Proton motive force drives the  
563 interaction of the inner membrane TolA and outer membrane pal proteins in Escherichia coli."  
564 *Mol Microbiol* **38**(4): 904-915.

565 Cascales, E., R. Lloubès and J. N. Sturgis (2001). "The TolQ-TolR proteins energize TolA and  
566 share homologies with the flagellar motor proteins MotA-MotB." *Mol Microbiol* **42**(3): 795-  
567 807.

568 Celia, H., I. Botos, X. Ni, T. Fox, N. De Val, R. Lloubes, J. Jiang and S. K. Buchanan (2019).  
569 "Cryo-EM structure of the bacterial Ton motor subcomplex ExbB-ExbD provides information  
570 on structure and stoichiometry." *Commun Biol* **2**: 358.

571 Celia, H., N. Noinaj, S. D. Zakharov, E. Bordignon, I. Botos, M. Santamaria, T. J. Barnard, W.  
572 A. Cramer, R. Lloubes and S. K. Buchanan (2016). "Structural insight into the role of the Ton  
573 complex in energy transduction." *Nature* **538**(7623): 60-65.

574 Chen, S., M. G. Kaufman, M. Bagdasarian, A. K. Bates and E. D. Walker (2010). "Development  
575 of an efficient expression system for Flavobacterium strains." *Gene* **458**(1-2): 1-10.

576 Chen, Y. Y., B. Peng, Q. Yang, M. D. Glew, P. D. Veith, K. J. Cross, K. N. Goldie, D. Chen,  
577 N. O'Brien-Simpson, S. G. Dashper and E. C. Reynolds (2011). "The outer membrane protein  
578 LptO is essential for the O-deacylation of LPS and the co-ordinated secretion and attachment  
579 of A-LPS and CTD proteins in Porphyromonas gingivalis." *Mol Microbiol* **79**(5): 1380-1401.

580 Ducret, A., E. M. Quardokus and Y. V. Brun (2016). "MicrobeJ, a tool for high throughput  
581 bacterial cell detection and quantitative analysis." *Nature microbiology* **1**(7): 1-7.

582 Duxbury, T., B. A. Humphrey and K. Marshall (1980). "Continuous observations of bacterial  
583 gliding motility in a dialysis microchamber: the effects of inhibitors." *Archives of Microbiology*  
584 **124**(2-3): 169-175.

585 Dzink-Fox, J. L., E. R. Leadbetter and W. Godchaux (1997). "Acetate acts as a protonophore  
586 and differentially affects bead movement and cell migration of the gliding bacterium Cytophaga  
587 johnsonae (Flavobacterium johnsoniae)." *Microbiology* **143** ( Pt 12): 3693-3701.

588 Germon, P., M. C. Ray, A. Vianney and J. C. Lazzaroni (2001). "Energy-dependent  
589 conformational change in the TolA protein of Escherichia coli involves its N-terminal domain,  
590 TolQ, and TolR." *J Bacteriol* **183**(14): 4110-4114.

591 Glew, M. D., P. D. Veith, D. Chen, D. G. Gorasia, B. Peng and E. C. Reynolds (2017). "PorV  
592 is an Outer Membrane Shuttle Protein for the Type IX Secretion System." *Sci Rep* **7**(1): 8790.

593 Glew, M. D., P. D. Veith, B. Peng, Y. Y. Chen, D. G. Gorasia, Q. Yang, N. Slakeski, D. Chen,  
594 C. Moore, S. Crawford and E. C. Reynolds (2012). "PG0026 is the C-terminal signal peptidase  
595 of a novel secretion system of Porphyromonas gingivalis." *J Biol Chem* **287**(29): 24605-24617.

596 Gorasia, D., G. Chreifi, C. Seers, C. Butler, J. Heath, M. Glew, M. McBride, P. Subramanian,  
597 A. Kjær, G. Jensen, P. Veith and E. Reynolds (2020). "In situ structure and organisation of the  
598 type IX secretion system." *bioRxiv*: 2020.2005.2013.094771.

599 Gorasia, D. G., P. D. Veith, D. Chen, C. A. Seers, H. A. Mitchell, Y. Y. Chen, M. D. Glew, S.  
600 G. Dashper and E. C. Reynolds (2015). "Porphyromonas gingivalis Type IX Secretion  
601 Substrates Are Cleaved and Modified by a Sortase-Like Mechanism." *PLoS Pathog* **11**(9):  
602 e1005152.

603 Gorasia, D. G., P. D. Veith, E. G. Hanssen, M. D. Glew, K. Sato, H. Yukitake, K. Nakayama  
604 and E. C. Reynolds (2016). "Structural Insights into the PorK and PorN Components of the  
605 Porphyromonas gingivalis Type IX Secretion System." *PLoS Pathog* **12**(8): e1005820.

606 Gorasia, D. G., P. D. Veith and E. C. Reynolds (2020). "The Type IX Secretion System:  
607 Advances in Structure, Function and Organisation." *Microorganisms* **8**(8).

608 Goulas, T., D. Mizgalska, I. Garcia-Ferrer, T. Kantyka, T. Guevara, B. Szmigielski, A. Sroka,  
609 C. Millán, I. Usón, F. Veillard, B. Potempa, P. Mydel, M. Solà, J. Potempa and F. X. Gomis-  
610 Rùth (2015). "Structure and mechanism of a bacterial host-protein citrullinating virulence  
611 factor, Porphyromonas gingivalis peptidylarginine deiminase." *Sci Rep* **5**: 11969.

612 Götzke, H., M. Kilisch, M. Martínez-Carranza, S. Sograte-Idrissi, A. Rajavel, T. Schlichthaerle,  
613 N. Engels, R. Jungmann, P. Stenmark, F. Opazo and S. Frey (2019). "The ALFA-tag is a highly  
614 versatile tool for nanobody-based bioscience applications." *Nat Commun* **10**(1): 4403.  
615 Hennell James, R., J. C. Deme, A. Kjær, F. Alcock, A. Silale, F. Lauber, S. Johnson, B. C.  
616 Berks and S. M. Lea (2021). "Structure and mechanism of the proton-driven motor that powers  
617 type 9 secretion and gliding motility." *Nat Microbiol* **6**(2): 221-233.  
618 Julius, A., L. Laur, C. Schanzenbach and D. Langosch (2017). "BLaTM 2.0, a genetic tool  
619 revealing preferred antiparallel interaction of transmembrane helix 4 of the dual-topology  
620 protein EmrE." *Journal of molecular biology* **429**(11): 1630-1637.  
621 Kharade, S. S. and M. J. McBride (2014). "Flavobacterium johnsoniae chitinase ChiA is  
622 required for chitin utilization and is secreted by the type IX secretion system." *J Bacteriol*  
623 **196**(5): 961-970.  
624 Khorana, H. G. (1953). "The Chemistry of Carbodiimides." *Chemical Reviews* **53**(2): 145-166.  
625 Kim, E. A., M. Price-Carter, W. C. Carlquist and D. F. Blair (2008). "Membrane segment  
626 organization in the stator complex of the flagellar motor: implications for proton flow and  
627 proton-induced conformational change." *Biochemistry* **47**(43): 11332-11339.  
628 Kita, D., S. Shibata, Y. Kikuchi, E. Kokubu, K. Nakayama, A. Saito and K. Ishihara (2016).  
629 "Involvement of the Type IX Secretion System in Capnocytophaga ochracea Gliding Motility  
630 and Biofilm Formation." *Appl Environ Microbiol* **82**(6): 1756-1766.  
631 Kojima, S. and D. F. Blair (2001). "Conformational change in the stator of the bacterial flagellar  
632 motor." *Biochemistry* **40**(43): 13041-13050.  
633 Kulkarni, S. S., J. J. Johnston, Y. Zhu, Z. T. Hying and M. J. McBride (2019). "The Carboxy-  
634 Terminal Region of Flavobacterium johnsoniae SprB Facilitates Its Secretion by the Type IX  
635 Secretion System and Propulsion by the Gliding Motility Machinery." *J Bacteriol* **201**(19).  
636 Larsen, R. A., M. G. Thomas and K. Postle (1999). "Protonmotive force, ExbB and ligand-  
637 bound FepA drive conformational changes in TonB." *Mol Microbiol* **31**(6): 1809-1824.  
638 Lasica, A. M., M. Ksiazek, M. Madej and J. Potempa (2017). "The Type IX Secretion System  
639 (T9SS): Highlights and Recent Insights into Its Structure and Function." *Front Cell Infect*  
640 *Microbiol* **7**: 215.  
641 Lauber, F., J. C. Deme, S. M. Lea and B. C. Berks (2018). "Type 9 secretion system structures  
642 reveal a new protein transport mechanism." *Nature* **564**(7734): 77-82.  
643 Leone, P., J. Roche, M. S. Vincent, Q. H. Tran, A. Desmyter, E. Cascales, C. Kellenberger, C.  
644 Cambillau and A. Roussel (2018). "Type IX secretion system PorM and gliding machinery  
645 GldM form arches spanning the periplasmic space." *Nat Commun* **9**(1): 429.  
646 Liu, J., M. J. McBride and S. Subramaniam (2007). "Cell surface filaments of the gliding  
647 bacterium Flavobacterium johnsoniae revealed by cryo-electron tomography." *J Bacteriol*  
648 **189**(20): 7503-7506.  
649 Logger, L., A. Zoued and E. Cascales (2017). "Fusion Reporter Approaches to Monitoring  
650 Transmembrane Helix Interactions in Bacterial Membranes." *Methods Mol Biol* **1615**: 199-  
651 210.  
652 Lunar Silva, I. and E. Cascales (2021). "Molecular Strategies Underlying Porphyromonas  
653 gingivalis Virulence." *J Mol Biol* **433**(7): 166836.  
654 Madej, M., Z. Nowakowska, M. Ksiazek, A. M. Lasica, D. Mizgalska, M. Nowak, A. Jacula,  
655 M. Bzowska, C. Scavenius, J. J. Enghild, J. Aduse-Opoku, M. A. Curtis, F. X. Gomis-Rüth and  
656 J. Potempa (2021). "PorZ, an Essential Component of the Type IX Secretion System of  
657 Porphyromonas gingivalis, Delivers Anionic Lipopolysaccharide to the PorU Sortase for  
658 Transpeptidase Processing of T9SS Cargo Proteins." *mBio* **12**(1).  
659 McBride, M. J. (2019). "Gliding Motility and the Type IX Secretion System." *Microbiol Spectr*  
660 **7**(1).



- 661 McBride, M. J. and M. J. Kempf (1996). "Development of techniques for the genetic  
662 manipulation of the gliding bacterium *Cytophaga johnsonae*." J Bacteriol **178**(3): 583-590.
- 663 McBride, M. J. and Y. Zhu (2013). "Gliding motility and Por secretion system genes are  
664 widespread among members of the phylum bacteroidetes." J Bacteriol **195**(2): 270-278.
- 665 Nakane, D., K. Sato, H. Wada, M. J. McBride and K. Nakayama (2013). "Helical flow of  
666 surface protein required for bacterial gliding motility." Proc Natl Acad Sci U S A **110**(27):  
667 11145-11150.
- 668 Nakayama, K. (2015). "Porphyromonas gingivalis and related bacteria: from colonial  
669 pigmentation to the type IX secretion system and gliding motility." J Periodontal Res **50**(1): 1-  
670 8.
- 671 Nan, B., M. J. McBride, J. Chen, D. R. Zusman and G. Oster (2014). "Bacteria that glide with  
672 helical tracks." Curr Biol **24**(4): R169-173.
- 673 Nan, B. and D. R. Zusman (2016). "Novel mechanisms power bacterial gliding motility." Mol  
674 Microbiol **101**(2): 186-193.
- 675 Nelson, S. S., S. Bollampalli and M. J. McBride (2008). "SprB is a cell surface component of  
676 the *Flavobacterium johnsoniae* gliding motility machinery." J Bacteriol **190**(8): 2851-2857.
- 677 Pate, J. L. and L.-Y. E. Chang (1979). "Evidence that gliding motility in prokaryotic cells is  
678 driven by rotary assemblies in the cell envelopes." Current Microbiology **2**(1): 59-64.
- 679 Rath, A., M. Glibowicka, V. G. Nadeau, G. Chen and C. M. Deber (2009). "Detergent binding  
680 explains anomalous SDS-PAGE migration of membrane proteins." Proceedings of the National  
681 Academy of Sciences **106**(6): 1760-1765.
- 682 Rhodes, R. G., H. G. Pucker and M. J. McBride (2011). "Development and use of a gene  
683 deletion strategy for *Flavobacterium johnsoniae* to identify the redundant gliding motility genes  
684 *remF*, *remG*, *remH*, and *remI*." J Bacteriol **193**(10): 2418-2428.
- 685 Rhodes, R. G., M. N. Samarasam, A. Shrivastava, J. M. van Baaren, S. Pochiraju, S.  
686 Bollampalli and M. J. McBride (2010). "*Flavobacterium johnsoniae* *gldN* and *gldO* are partially  
687 redundant genes required for gliding motility and surface localization of SprB." J Bacteriol  
688 **192**(5): 1201-1211.
- 689 Ridgway, H. F. (1977). "Source of energy for gliding motility in *Flexibacter polymorphus*:  
690 effects of metabolic and respiratory inhibitors on gliding movement." J Bacteriol **131**(2): 544-  
691 556.
- 692 Santiveri, M., A. Roa-Eguiara, C. Kühne, N. Wadhwa, H. Hu, H. C. Berg, M. Erhardt and N.  
693 M. I. Taylor (2020). "Structure and Function of Stator Units of the Bacterial Flagellar Motor." Cell  
694 **183**(1): 244-257.e216.
- 695 Sato, K., M. Naito, H. Yukitake, H. Hirakawa, M. Shoji, M. J. McBride, R. G. Rhodes and K.  
696 Nakayama (2010). "A protein secretion system linked to bacteroidete gliding motility and  
697 pathogenesis." Proc Natl Acad Sci U S A **107**(1): 276-281.
- 698 Sato, K., K. Okada, K. Nakayama and K. Imada (2020). "PorM, a core component of bacterial  
699 type IX secretion system, forms a dimer with a unique kinked-rod shape." Biochem Biophys  
700 Res Commun **532**(1): 114-119.
- 701 Schanzenbach, C., F. C. Schmidt, P. Breckner, M. G. Teese and D. Langosch (2017).  
702 "Identifying ionic interactions within a membrane using BLaTM, a genetic tool to measure  
703 homo- and heterotypic transmembrane helix-helix interactions." Scientific reports **7**: 43476.
- 704 Schneider, D. and D. M. Engelman (2003). "GALLEX, a measurement of heterologous  
705 association of transmembrane helices in a biological membrane." Journal of Biological  
706 Chemistry **278**(5): 3105-3111.
- 707 Shrivastava, A. and H. C. Berg (2020). "A molecular rack and pinion actuates a cell-surface  
708 adhesin and enables bacterial gliding motility." Sci Adv **6**(10): eaay6616.



- 709 Shrivastava, A., J. J. Johnston, J. M. van Baaren and M. J. McBride (2013). "Flavobacterium  
710 johnsoniae GldK, GldL, GldM, and SprA are required for secretion of the cell surface gliding  
711 motility adhesins SprB and RemA." J Bacteriol **195**(14): 3201-3212.
- 712 Shrivastava, A., P. P. Lele and H. C. Berg (2015). "A rotary motor drives Flavobacterium  
713 gliding." Curr Biol **25**(3): 338-341.
- 714 Shrivastava, A., R. G. Rhodes, S. Pochiraju, D. Nakane and M. J. McBride (2012).  
715 "Flavobacterium johnsoniae RemA is a mobile cell surface lectin involved in gliding." J  
716 Bacteriol **194**(14): 3678-3688.
- 717 Shrivastava, A., T. Roland and H. C. Berg (2016). "The Screw-Like Movement of a Gliding  
718 Bacterium Is Powered by Spiral Motion of Cell-Surface Adhesins." Biophys J **111**(5): 1008-  
719 1013.
- 720 Skare, J. T. and K. Postle (1991). "Evidence for a TonB-dependent energy transduction  
721 complex in Escherichia coli." Mol Microbiol **5**(12): 2883-2890.
- 722 Song, L., D. J. Perpich, C. Wu, T. Doan, J. Potempa, J. P. Christie, E. Cascales, J. R. Lamont  
723 and B. Hu (2021). "A Unique Bacterial Secretion Machinery with Multiple Secretion Centers."  
724 Sun, M., M. Wartel, E. Cascales, J. W. Shaevitz and T. Mignot (2011). "Motor-driven  
725 intracellular transport powers bacterial gliding motility." Proc Natl Acad Sci U S A **108**(18):  
726 7559-7564.
- 727 Tinevez, J.-Y., N. Perry, J. Schindelin, G. M. Hoopes, G. D. Reynolds, E. Laplantine, S. Y.  
728 Bednarek, S. L. Shorte and K. W. Eliceiri (2017). "TrackMate: An open and extensible platform  
729 for single-particle tracking." Methods **115**: 80-90.
- 730 Togashi, F., S. Yamaguchi, M. Kihara, S.-I. Aizawa and R. M. Macnab (1997). "An extreme  
731 clockwise switch bias mutation in fliG of Salmonella typhimurium and its suppression by slow-  
732 motile mutations in motA and motB." Journal of Bacteriology **179**(9): 2994-3003.
- 733 Tomek, M. B., L. Neumann, I. Nimeth, A. Koerdt, P. Andesner, P. Messner, L. Mach, J. S.  
734 Potempa and C. Schäffer (2014). "The S-layer proteins of Tannerella forsythia are secreted via  
735 a type IX secretion system that is decoupled from protein O-glycosylation." Mol Oral Microbiol  
736 **29**(6): 307-320.
- 737 Vincent, M. S., M. J. Canestrari, P. Leone, J. Stathopoulos, B. Ize, A. Zoued, C. Cambillau, C.  
738 Kellenberger, A. Roussel and E. Cascales (2017). "Characterization of the." J Biol Chem  
739 **292**(8): 3252-3261.
- 740 Vincent, M. S., M. J. Canestrari, P. Leone, J. Stathopoulos, B. Ize, A. Zoued, C. Cambillau, C.  
741 Kellenberger, A. Roussel and E. Cascales (2017). "Characterization of the Porphyromonas  
742 gingivalis Type IX Secretion Trans-envelope PorKLMNP Core Complex." J Biol Chem **292**(8):  
743 3252-3261.
- 744 Wadhwa, N. and H. C. Berg (2021). "Bacterial motility: machinery and mechanisms." Nat Rev  
745 Microbiol.
- 746 Wartel, M., A. Ducret, S. Thutupalli, F. Czerwinski, A. V. Le Gall, E. M. Mauriello, P. Bergam,  
747 Y. V. Brun, J. Shaevitz and T. Mignot (2013). "A versatile class of cell surface directional  
748 motors gives rise to gliding motility and sporulation in Myxococcus xanthus." PLoS Biol  
749 **11**(12): e1001728.
- 750 Zhang, X. Y., E. L. Goemaere, R. Thomé, M. Gavioli, E. Cascales and R. Lloubès (2009).  
751 "Mapping the interactions between escherichia coli tol subunits: rotation of the TolR  
752 transmembrane helix." J Biol Chem **284**(7): 4275-4282.
- 753 Zhou, J., L. L. Sharp, H. L. Tang, S. A. Lloyd, S. Billings, T. F. Braun and D. F. Blair (1998).  
754 "Function of protonatable residues in the flagellar motor of Escherichia coli: a critical role for  
755 Asp 32 of MotB." J Bacteriol **180**(10): 2729-2735.

756

## 757 Author Contributions

758 MSV, EC and TD conceived the study. MSV, CCH, CSK, HLG, MC, EC and TD contributed  
759 to experiments and data analysis, with the main contribution of MSV. AK, FG, TM and MM  
760 provided resources, technical and conceptual input. EC acquired funding. MSV, EC and TD  
761 wrote the original draft. CSK, MSV, EC and TD edited the manuscript with the help of other  
762 co-authors.

763

## 764 Legend to Figures

### 765 Figure 1 | Effects of PMF dissipating drugs on the gliding of *F. johnsoniae* cells. (A)

766 Rainbow traces of cell motility on glass recorded by phase contrast microscopy over time (2  
767 min) in the absence of drug or in the presence of CCCP, nigericin or valinomycin. Individual  
768 frames from time lapse acquisition were coloured from red (start) to yellow, green, cyan and  
769 blue (end) and merged into a single rainbow image. Scale bar, 20  $\mu\text{m}$ . (B) Combined jitter  
770 plots/boxplots of mean cell gliding velocity (in  $\mu\text{m}\cdot\text{s}^{-1}$ ) of  $n>38$  wild-type cells before (-), during  
771 a pulse of 10  $\mu\text{M}$  CCCP (+CCCP), or 7  $\mu\text{M}$  nigericin (+Nig), or 40  $\mu\text{M}$  valinomycin/+50mM  
772 KCl (+Val), and after wash with fresh CYE medium (Wash). Statistical significance relative to  
773 the non-treated condition (-) is indicated above the plots (ns, non-significative; \*\*\*,  $p < 0.001$ ;  
774 Wilcoxon's  $t$ -test).

### 775 Figure 2 | Interactions between GldL and GldM transmembrane helices. (A) Bacterial two-

776 hybrid assay. GldL-GldM interaction is dependent on their TMHs. BTH101 cells producing the  
777 indicated proteins (GldL, GldM) or domains (GldL<sub>C</sub>, cytoplasmic domain of GldL, amino-acid  
778 59 to 189; GldM<sub>P</sub>, periplasmic domain of GldM, amino-acid 36 to 513) fused to the T18 and  
779 T25 domain of the *Bordetella* adenylate cyclase were spotted on X-Gal-IPTG reporter LB agar  
780 plates. The blue color of the colony reports interaction between the two partners. Controls  
781 include T18 and T25 fusions to TolB and Pal, two proteins that interact but unrelated to the  
782 T9SS. (B) Schematic representation of GldL and GldM domains and topologies in the IM. The  
783 GldL TMH1 (L1, blue) and TMH2 (L2, brown), and GldM TMH (M, green) are indicated. (C)  
784 Homo- and heterodimerization of *in-to-out* TMHs of GldL and GldM probed with the GALLEX  
785 method. Jitter plots of  $\beta$ -galactosidase activity reporting the dimerization of TMHs fused to  
786 LexA<sup>WT</sup> or LexA<sup>408</sup>. Measurements are reported as 1/ $\beta$ -galactosidase activity. Data are

787 combined from technical triplicates of four independent measurements (2 colonies from two  
788 independent transformations each). Interactions with TssL1 (in grey) served as negative  
789 controls. TssL1 is the TMH of TssL, a protein of the *E. coli* Type VI secretion system (T6SS)  
790 that homodimerizes. **(D)** Homo and heterodimerization of the *in-to-out* and *out-to-in* THMs of  
791 GldL and GldM probed with the BLA method. Jitter plots of CENTA chromogenic substrate  
792 hydrolysis after 10 min of incubation. The activity is reported as the  $A_{405\text{nm}}$  value per  $A_{600\text{nm}}$ .  
793 Controls include interaction assays with the TMHs of TssM (TssM1 and TssM2, in grey), a  
794 subunit of the *E. coli* T6SS.

795

796 **Figure 3 | Conformational changes in GldM periplasmic domain in response to the proton**  
797 **gradient. (A)** GldM protease accessibility assay. Spheroplasts of wild-type *F. johnsoniae* or  
798 the  $\Delta\text{gldM}$  mutant were treated (+) or not (-) with the trypsin protease and 10  $\mu\text{M}$  CCCP (PMF  
799 inhibitor), 7  $\mu\text{M}$  nigericin ( $\Delta\text{pH}$  inhibitor), 40  $\mu\text{M}$  valinomycin/ $\text{K}^+$  ( $\Delta\phi$  inhibitor), 1.5 mM  
800 sodium azide, or 20 mM sodium arsenate ( $\text{F}_1\text{F}_0$  ATPase inhibitors). GldM was analyzed by  
801 SDS-PAGE and immunoblot with anti-GldM antibodies. The full-length GldM protein is  
802 indicated, as well as degradation products (\* and \*\*). The molecular weight markers (in kDa)  
803 are indicated on the left. **(B)** Schematic model of GldM conformational transition dependent on  
804 the proton gradient.

805

806 **Figure 4 | Roles of conserved GldL TMH2 glutamates in T9SS-dependent secretion and**  
807 **dynamics of SprB. (A)** The addition of the drug DCCD inhibited cell motility. Rainbow traces  
808 of cell motility on glass recorded by phase contrast microscopy over time (2 min) in the  
809 presence of 10  $\mu\text{M}$  DCCD. **(B)** Combined jitter plots/boxplots of mean cell gliding velocity (in  
810  $\mu\text{m}\cdot\text{s}^{-1}$ ) of  $n > 50$  wild-type cells before (-), during a pulse of 10  $\mu\text{M}$  DCCD (+DCCD) and after  
811 wash with fresh CYE medium (Wash). Statistical significance relative to the non-treated  
812 condition (-) is indicated above the plots (ns, non-significant, \*\*\*,  $p < 0.001$ ; Wilcoxon's  $t$ -  
813 test). **(C)** Effect of DCCD on GldM protease susceptibility. GldM protease accessibility assay  
814 on spheroplasts of wild-type *F. johnsoniae* in absence (-) or presence (+) of 10  $\mu\text{M}$  DCCD. **(D)**  
815 GldM conserved glutamate 31 does not play an important role in gliding motility. Combined  
816 jitter plots/boxplots of mean cell gliding velocity (in  $\mu\text{m}\cdot\text{s}^{-1}$ ) of wild-type cells (WT,  $n=50$ ), and  
817 strains expressing ectopically  $\text{gldM}^{\text{WT}}$  ( $n=49$ ) or  $\text{gldM}^{\text{E31A}}$  point mutant ( $n=18$ ) in a  $\Delta\text{gldM}$   
818 mutant background. The  $\Delta\text{gldM}$  mutant has been placed in the graph for relevance but cell  
819 velocity has not been measured for that strain because it did not adhere to glass. **(E)** Combined

820 jitter plots/boxplots of mean cell gliding velocity (in  $\mu\text{m}\cdot\text{s}^{-1}$ ) of wild-type cells (WT, n=50) and  
821 a *gldL*<sup>E59A</sup> point mutant (n=26). Strains were cultivated in CYE and single-cell gliding was  
822 observed on a free glass coverslip by phase contrast microscopy during 2 min. Gliding of the  
823  $\Delta$ *gldL* mutant and of the *gldL*<sup>E49A</sup> point mutant was not measured because cells did not adhere  
824 to the glass substratum. **(F)** Localization and dynamics of SprB on the cell surface in the wild-  
825 type strain (WT), a  $\Delta$ *gldL* mutant, a *gldL*<sup>E49A</sup> point mutant and a *gldL*<sup>E59A</sup> point mutant. A  
826 representative cell is shown. Strains were cultured in CYE and, after SprB immunolabeling,  
827 were sandwiched between an agarose pad and a glass coverslip to significantly limit cell  
828 movement and facilitate SprB signal acquisition and analysis. SprB was immunolabeled using  
829 a primary serum directed against SprB and Alexa-488 fluorescent secondary antibodies.  
830 Fluorescence was recorded with 100 ms intervals for several seconds. The brightfield image  
831 (top panel), the first frame (middle panel, in grey levels) and the rainbow trace of SprB motion  
832 over time (bottom panel, not available for the  $\Delta$ *gldL* mutant and the *gldL*<sup>E49A</sup> point mutant) are  
833 shown. Scale bar, 2  $\mu\text{m}$ . **(G)** Combined jitter plots/boxplots of mean displacement velocity (in  
834  $\mu\text{m}\cdot\text{s}^{-1}$ ) of SprB in wild-type cells (WT, n=69) and a *gldL*<sup>E59A</sup> point mutant (n=85). SprB  
835 fluorescent spots were detected and tracked over time (>2 s) using the Trackmate plugin. **(H)**  
836 GldM protease accessibility assay in wild-type *F. johnsoniae* (WT), the  $\Delta$ *gldL* mutant, and  
837 GldL<sup>E49A</sup> and GldL<sup>E59A</sup> point mutants. Spheroplasts were treated with (+) or not (-) with the  
838 trypsin protease. GldM was analyzed by SDS-PAGE and immunoblot with anti-GldM  
839 antibodies. The full-length GldM protein is indicated, as well as degradation products (\* and  
840 \*\*). The molecular weight markers (in kDa) are indicated on the left.

841

842 **Figure 5 | GldL glutamate residues protonation probed by NMR.** pKa determination of <sup>13</sup>C-  
843 Glu of free and complexed L2 peptide. **(A)** 2D <sup>13</sup>C-HSQC spectra of 1 mM L2 peptide (<sup>13</sup>C-  
844 Glu labelled) in 150 mM deuterated DPC in 50 mM phosphate buffers at different pH (pH 2.9  
845 (yellow), 5.0 (orange), 5.8 (red), 6.7 (brown)). **(B)** The pH dependent chemical shift variations  
846 of C<sub>γ</sub> carbons of E49 and E59 of the L2 peptide free, or complexed with L1 and M in a 1:1:1  
847 molar ratio, were measured, fitted, and apparent pKa values were calculated using the  
848 Henderson-Hasselbach equation. **(C)** 2D <sup>13</sup>C-HSQC spectra of 1 mM L2 peptide (<sup>13</sup>C-Glu  
849 labelled) in 150 mM deuterated DPC in 50 mM phosphate buffer at pH 5.2 (left panel) and pH  
850 6.7 (right panel), in the absence (brown) and presence at molar ratio 1:1 of GldL-TMH1 peptide  
851 (L1, orange), GldM-TMH peptide (M, blue) and both L1 and M peptides (green).

852

853 **Figure 6 | Dynamic localization of Gld complexes. (A)** Localization of Gld proteins in fixed  
854 cells. Immunostaining of GldL, GldM, GldK and GldN and observation by structured-  
855 illumination microscopy. A typical specificity control is shown on the right panel with a  $\Delta gldM$   
856 mutant stained with antibodies directed against GldM. Scale bar 2  $\mu\text{m}$ . The number of foci was  
857 quantified for GldL- $\alpha$  and shown in a boxplot. **(B)** Live-cell dynamics of a functional GldL-  
858  $\alpha$  fusion bound to NbAlfa-sfGFP. After NbAlfa-sfGFP induction, GldL- $\alpha$  dynamics was  
859 followed by time lapse fluorescence microscopy with 300 ms intervals. For a representative  
860 cell, a stack of individual frames is shown. Time is indicated in ms. At the bottom of the stack,  
861 a kymograph of the fluorescence signal in the same representative cell. The x-axis is the  
862 position of GldL- $\alpha$ /NbAlfa-sfGFP signal with respect to the substratum (glass), and the y-  
863 axis is time. The red arrow shows an example of a static signal and the yellow arrow points to  
864 an example of a moving GldL- $\alpha$  focus. Scale bar 2  $\mu\text{m}$ . **(C)** GldL- $\alpha$  does not travel long  
865 distance within the cell. Diffusion of GldL- $\alpha$ /NbAlfa-sfGFP fluorescence signal over time  
866 assayed by FRAP. Cells expressing GldL- $\alpha$  and NbAlfa-sfGFP were pulse-bleached in the  
867 region indicated by the blue rectangle. A representative cell is shown. Scale bar 2  $\mu\text{m}$ . **(D)**  
868 Fluorescence intensities were measured in the bleached region (blue rectangle) and a non-  
869 bleached region (red rectangle) for 60 sec in 4 cells. Individual measurements are shown with  
870 spots (filled spots for bleached regions and empty spots for non-bleached regions). The green  
871 arrow indicates the moment of bleaching. The fluorescence intensity of each region of interest  
872 was normalized to the first prebleached intensity. The blue (bleached region) and red (non-  
873 bleached) lines indicate the average of all measurements. **(E)** GldL- $\alpha$  and SprB do not  
874 colocalize. Dynamic localization of GldL- $\alpha$  bound to NbAlfa-sfGFP (in green) and  
875 immunostained SprB (in red) in a representative cell. Fluorescence was followed by holo  
876 microscopy with 500 ms intervals. A stack of individual frames is shown. Time is indicated in  
877 ms. At the bottom of the stack, a kymograph of the fluorescence signal in the same  
878 representative cell. The x-axis is the position of the cell with respect to the substratum (glass),  
879 and the y-axis is time. Scale bar, 1  $\mu\text{m}$ . **(F)** Model of GldLM molecular motors function in Type  
880 IX secretion (top) and surface adhesin dynamics (bottom). GldLM motors (blue) are fueled by  
881 the proton gradient, leading to conformational shifts of the periplasmic domain of GldM. When  
882 associated to the T9SS (top), GldLM motors generate mechanical torque to rotate a GldKNO  
883 ring to drive secretion. GldLM motors may also be associated to the gliding machinery  
884 (bottom), in which they serve to transport SprB (in red) on the cell surface via the displacement



885 of a track or baseplate machinery (in green).

886

## 887 **Legend to Supplementary Figures**

888 **Supplementary Figure S1 | Network of interactions between proteins of the T9SS core**  
889 **components.** Bacterial two-hybrid assays. **(A)** T9SS outer membrane-associated core complex  
890 (GldK, GldN and GldO) and GldJ. **(B)** T9SS outer membrane-associated core complex (GldK,  
891 GldN, GldO), GldJ and the inner membrane-associated core complex (GldM, GldL). The signal  
892 sequence was omitted in the constructs for GldN and GldO. The signal sequence and the  
893 acylated N-terminal cysteine residue of the mature form were omitted for GldK and GldJ.  
894 BTH101 reporter cells producing the indicated proteins or domains (GldL<sub>C</sub>, cytoplasmic  
895 domain of the GldL protein; GldM<sub>P</sub>, periplasmic domain of the GldM protein) fused to the T18  
896 or T25 domain of the *Bordetella* adenylate cyclase were spotted on plates supplemented with  
897 IPTG and the chromogenic substrate X-Gal. The TolB-Pal interaction serves as positive control.  
898 **(C)** Model of the interactions between T9SS components defined by bacterial two-hybrid.

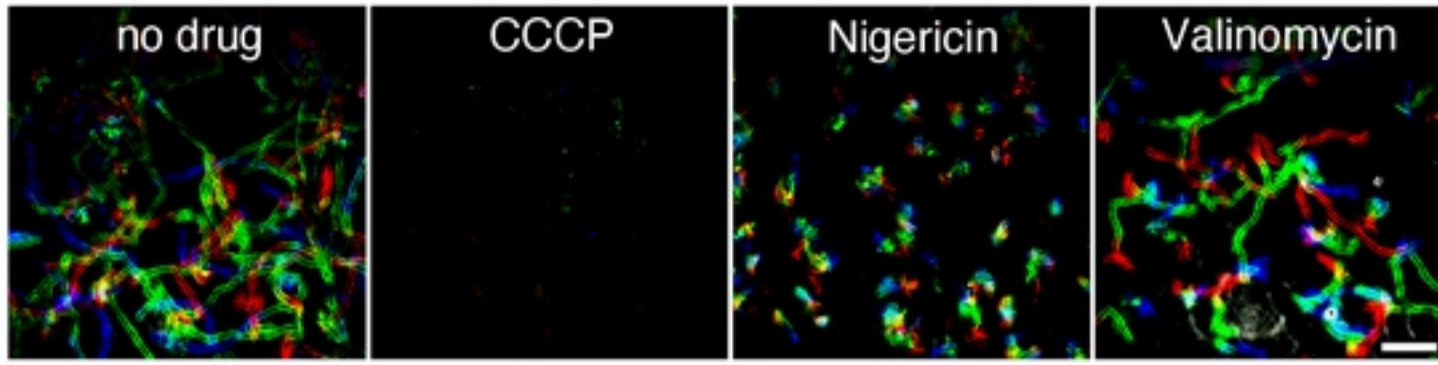
899 **Supplementary Figure S2 | (A)** Sequence alignments of the N-terminal regions that  
900 encompass the two transmembrane segments of GldL homologs. The alignment was performed  
901 using TCOFFEE. Red arrows indicate the conserved acidic residues. **(B)** Sequence alignments  
902 of the region that encompasses the single transmembrane segment of GldM homologs. The  
903 alignment was performed using TCOFFEE. The red arrow indicates the conserved acidic  
904 residue. **(C)** Highlight of GldL-E49 (orange) and E59 (pink) glutamate residues in the structural  
905 model of the GldLM complex. The left panel shows a side view and the right panel shows a  
906 view from the cytoplasm. GldL TMHs are colored green. GldM subunits (TMH and first  
907 periplasmic domain) are colored blue. **(D)** Western blot analysis of GldM production using anti-  
908 GldM antibodies in a  $\Delta gldM$  mutant, wild-type *F. johnsoniae* (WT), GldM WT or GldM E31A  
909 expressed from a plasmid in a  $\Delta gldM$  mutant background. **(E)** Western blot analysis of GldL  
910 production using anti-GldL antibodies in the  $\Delta gldL$  mutant ( $\Delta gldL$ ), wild-type *F. johnsoniae*  
911 (WT), and strains expressing GldL<sup>WT</sup>-flag (GldL<sup>WT</sup>) or GldL<sup>E49A</sup>-flag (E49A) or GldL<sup>E59A</sup>-flag  
912 (E59A). Extracts of cells were subjected to SDS-PAGE and immunodetection with anti-GldL  
913 and anti-Flag primary antibodies and HRP-coupled secondary antibodies. Molecular weight  
914 markers (in kDa) are indicated on left.

915 **Supplementary Figure S3 | GldL-alfa supports cell gliding.** **(A)** Rainbow traces of cell



916 motility on glass recorded by phase contrast microscopy over time (2 min) in a wild-type strain  
917 and a strain expressing *gldL-alfa* at the native locus. Individual frames from time lapse  
918 acquisition were coloured from red (start) to yellow, green, cyan and blue (end) and merged  
919 into a single rainbow image. Scale bar, 20  $\mu\text{m}$ . **(B)** Combined jitter plots/boxplots of mean cell  
920 gliding velocity (in  $\mu\text{m}\cdot\text{s}^{-1}$ ) of *gldL-alfa* cells in the absence of NbAlfa-sfGFP (-, n=124) or  
921 with 1 mM IPTG induction of NbAlfa-sfGFP (+, n=125) or wild-type cells in the absence of  
922 NbAlfa-sfGFP (-, n=135) or with 1 mM IPTG induction of NbAlfa-sfGFP (+, n=151). **(C)**  
923 Representative micrograph of cells expressing fluorescent NbAlfa-sfGFP in a wild-type  
924 background. Scale bar, 2  $\mu\text{m}$ .

A



B

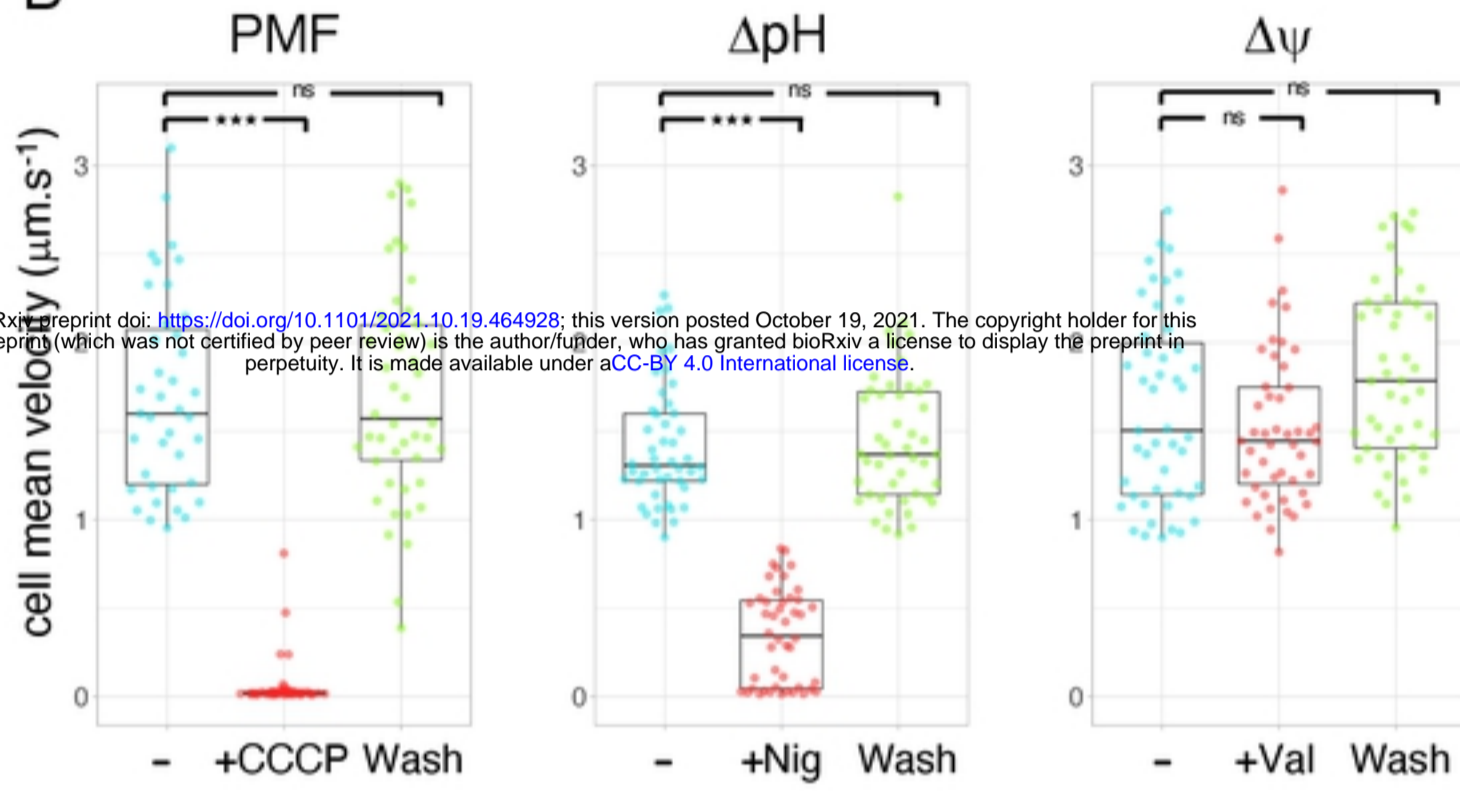
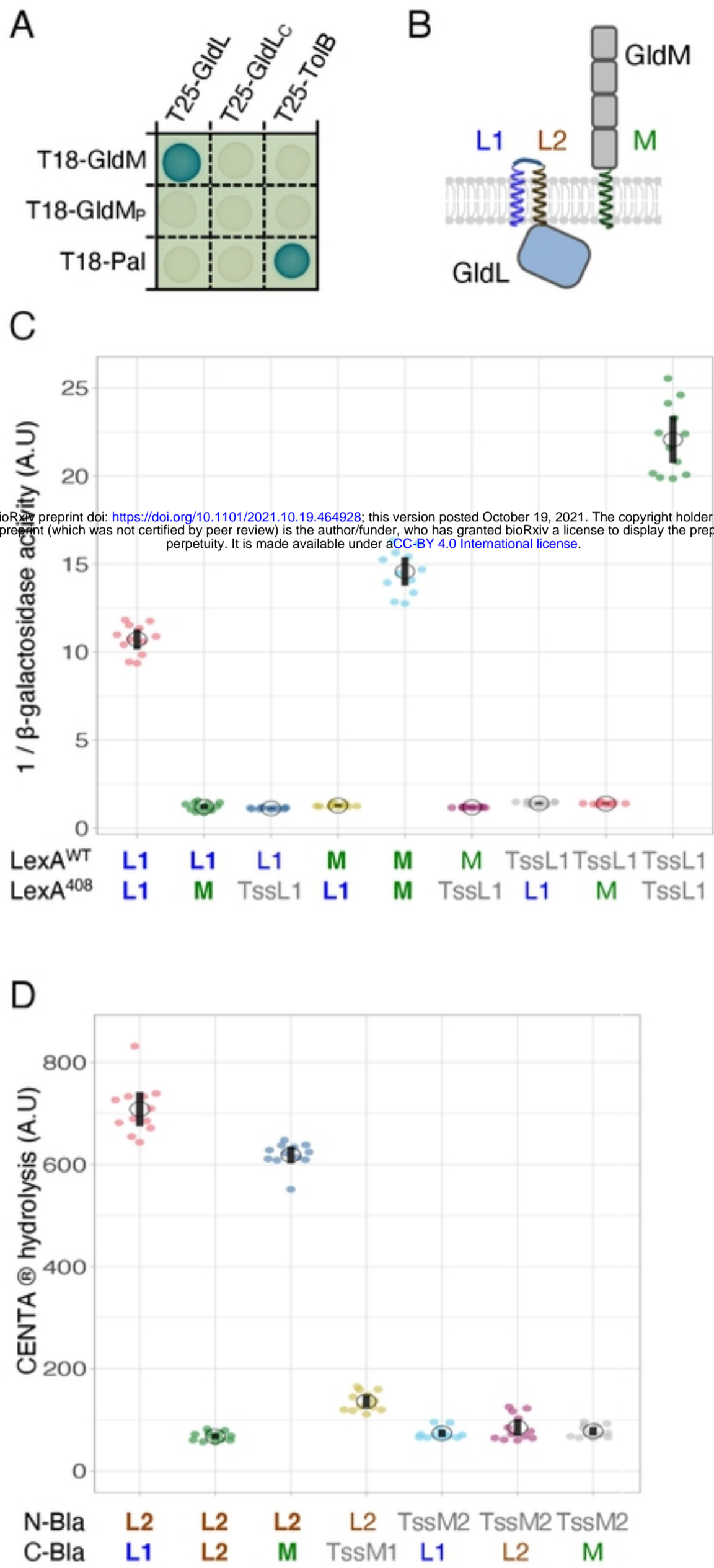
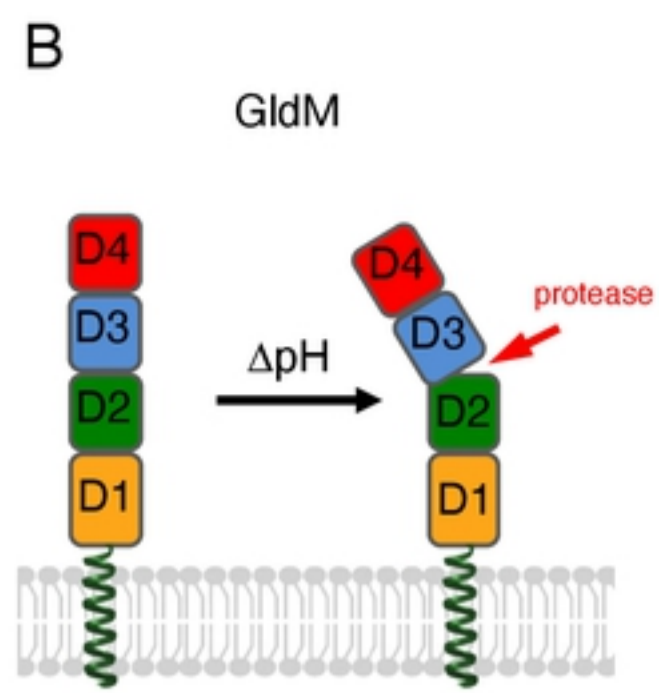
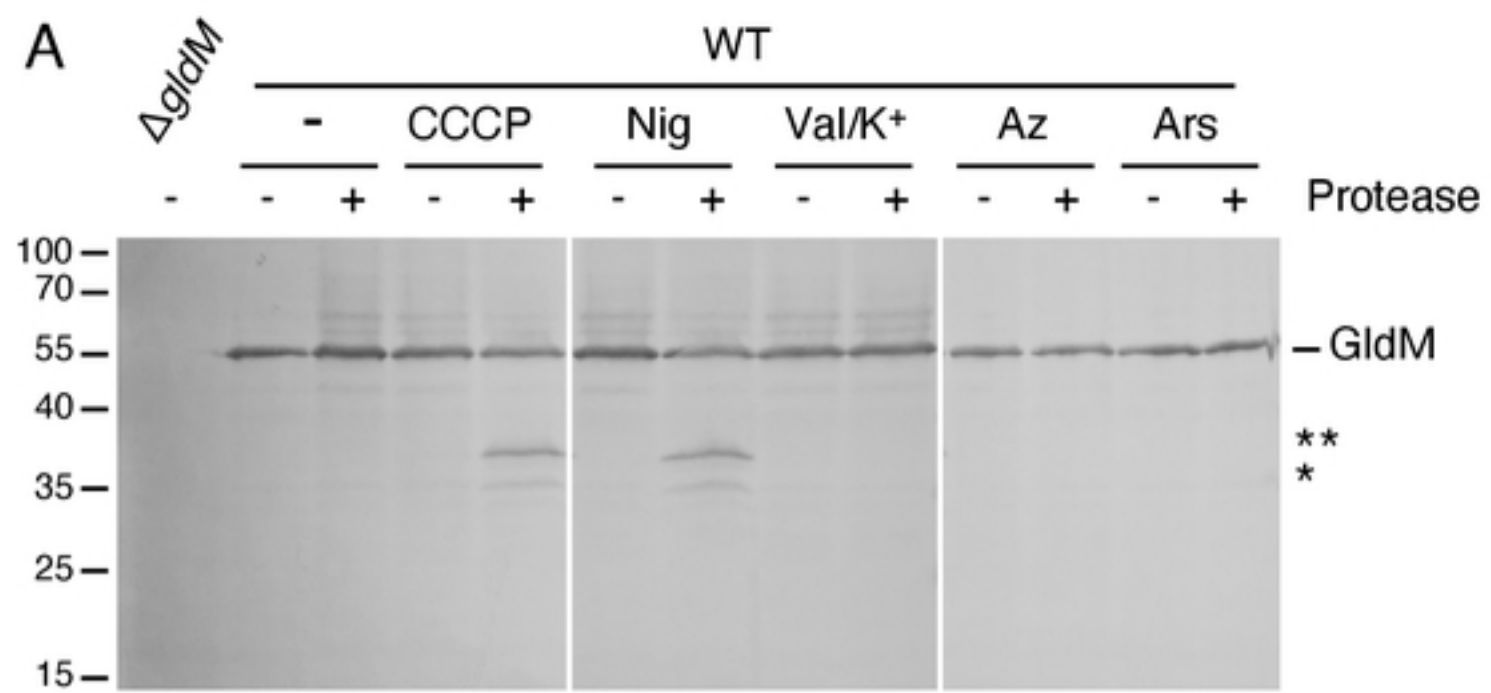


Figure 1



bioRxiv preprint doi: <https://doi.org/10.1101/2021.10.19.464928>; this version posted October 19, 2021. The copyright holder for this preprint (which was not certified by peer review) is the author/funder, who has granted bioRxiv a license to display the preprint in perpetuity. It is made available under aCC-BY 4.0 International license.

Figure 2



bioRxiv preprint doi: <https://doi.org/10.1101/2021.10.19.464928>; this version posted October 19, 2021. The copyright holder for this preprint (which was not certified by peer review) is the author/funder, who has granted bioRxiv a license to display the preprint in perpetuity. It is made available under aCC-BY 4.0 International license.

Figure 3

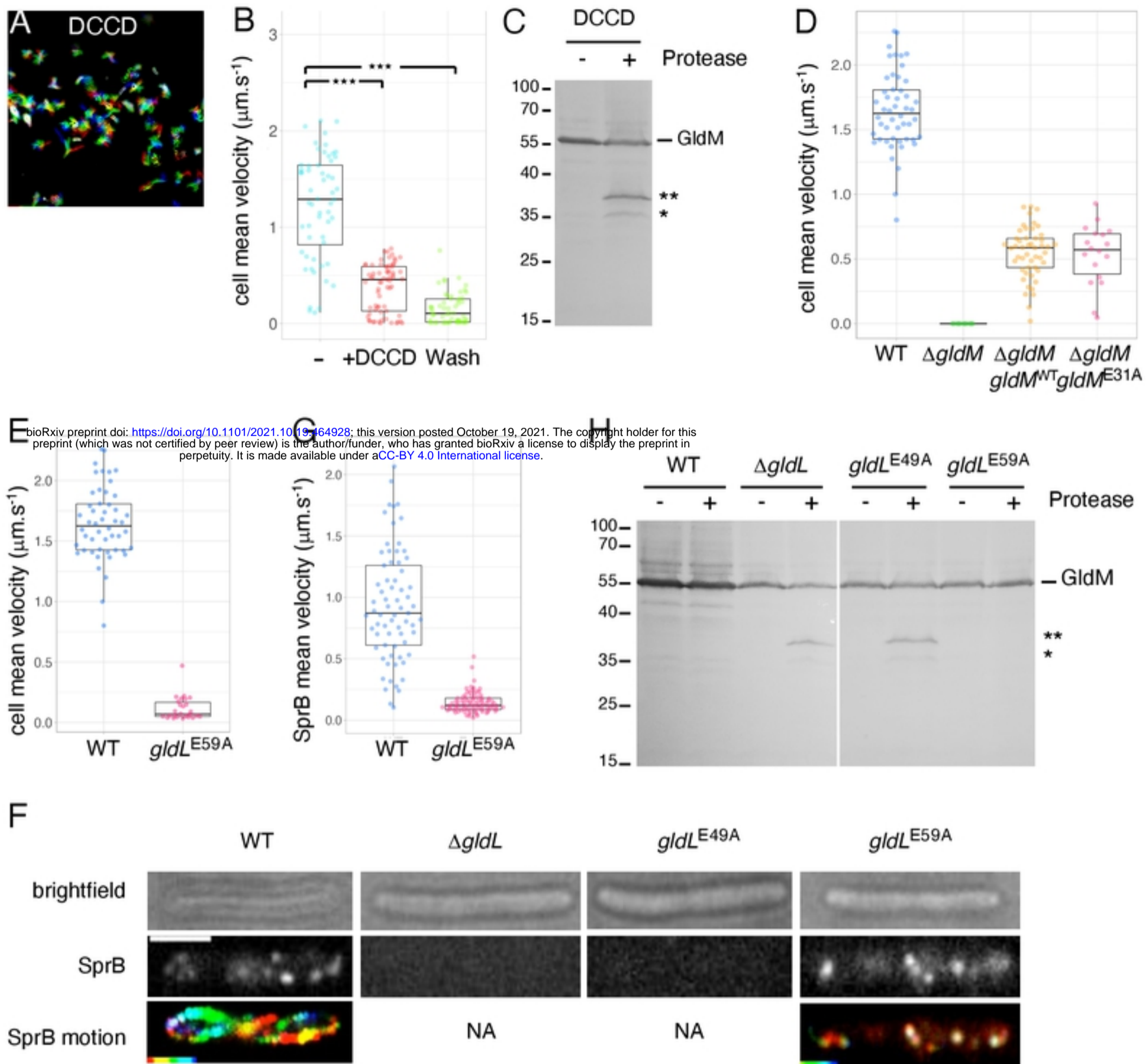


Figure 4



bioRxiv preprint doi: <https://doi.org/10.1101/2021.10.19.464928>; this version posted October 19, 2021. The copyright holder for this preprint (which was not certified by peer review) is the author/funder, who has granted bioRxiv a license to display the preprint in perpetuity. It is made available under aCC-BY 4.0 International license.

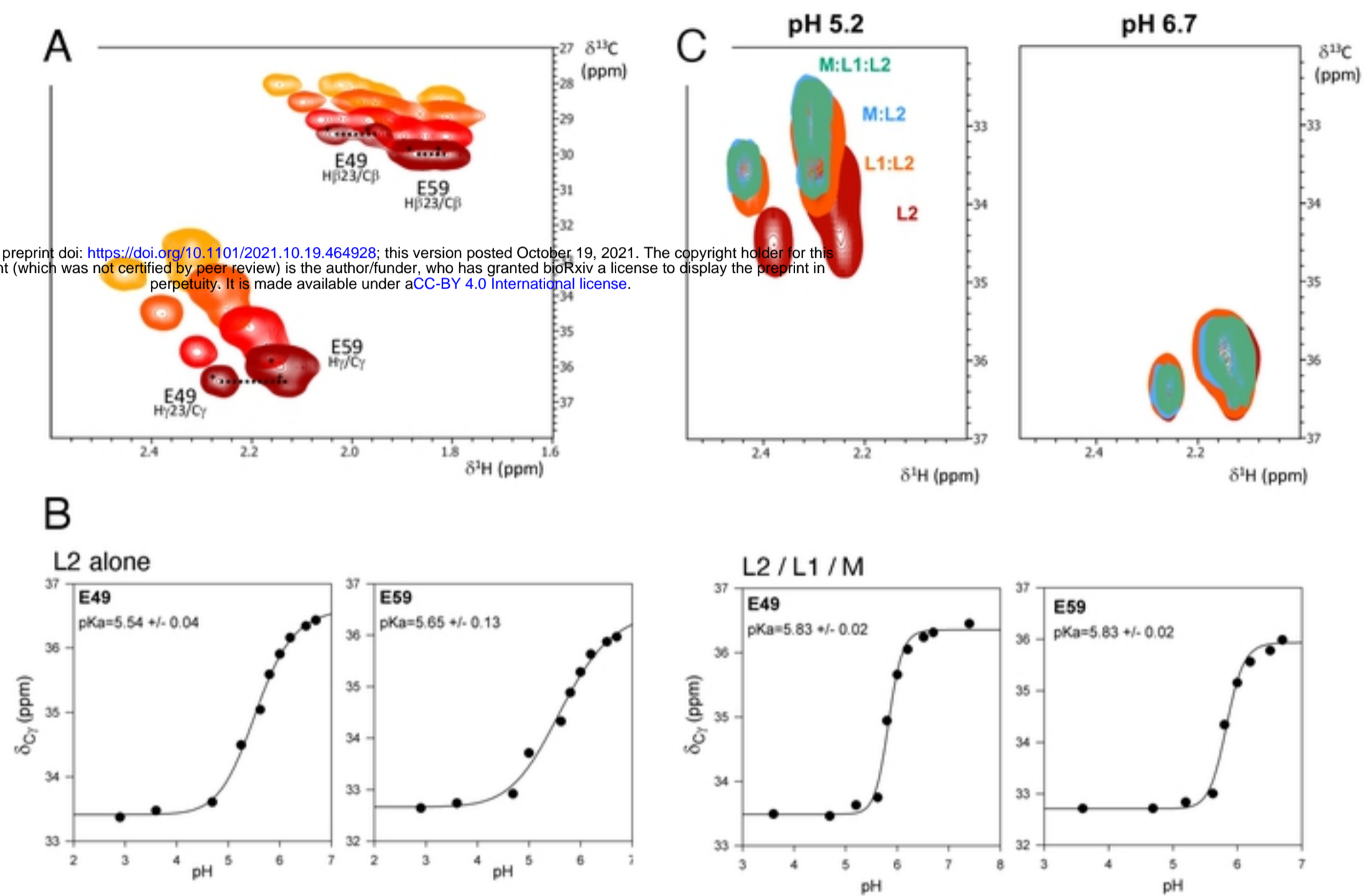


Figure 5

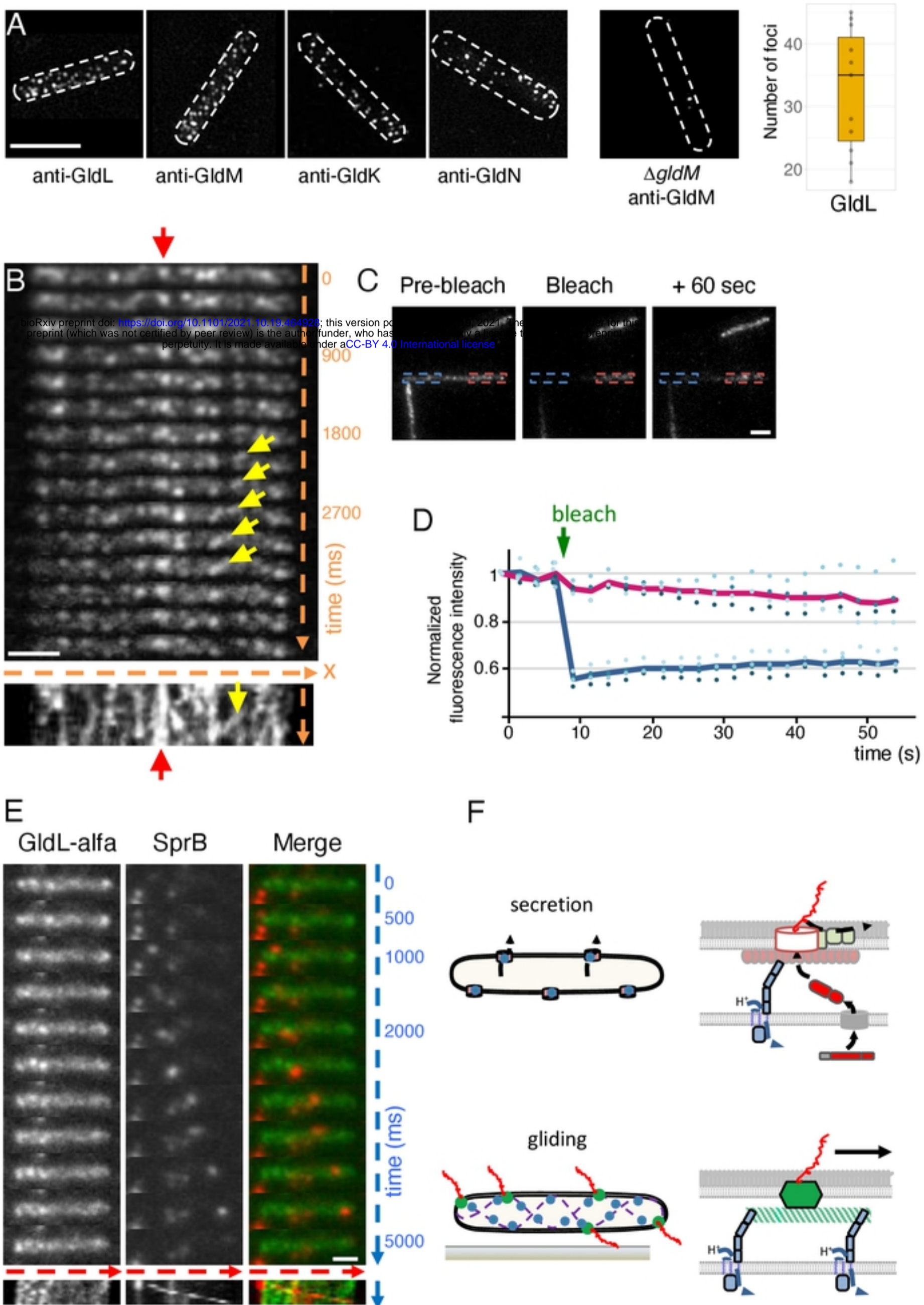


Figure 6